



LAWRENCE
LIVERMORE
NATIONAL
LABORATORY

Multiscale two-level solver for Biot's poroelasticity equations in subsurface media

S. Klevtsov, H. Hajibeygi, H. A. Tchelepi

March 15, 2018

Computational Geosciences

Disclaimer

This document was prepared as an account of work sponsored by an agency of the United States government. Neither the United States government nor Lawrence Livermore National Security, LLC, nor any of their employees makes any warranty, expressed or implied, or assumes any legal liability or responsibility for the accuracy, completeness, or usefulness of any information, apparatus, product, or process disclosed, or represents that its use would not infringe privately owned rights. Reference herein to any specific commercial product, process, or service by trade name, trademark, manufacturer, or otherwise does not necessarily constitute or imply its endorsement, recommendation, or favoring by the United States government or Lawrence Livermore National Security, LLC. The views and opinions of authors expressed herein do not necessarily state or reflect those of the United States government or Lawrence Livermore National Security, LLC, and shall not be used for advertising or product endorsement purposes.

Multiscale two-stage solver for Biot's poroelasticity equations in subsurface media

Nicola Castelletto^{1,2} · Sergey Klevtsov¹ · Hadi Hajibeygi³ · Hamdi A. Tchelepi¹

Abstract We propose a two-stage preconditioner for accelerating the iterative solution by a Krylov subspace method of Biot's poroelasticity equations based on a displacement-pressure formulation. The spatial discretization combines a finite-element method for mechanics and a finite-volume approach for flow. The fully-implicit backward Euler scheme is used for time integration. The result is a 2×2 block linear system for each timestep. The preconditioning operator is obtained by applying a two-stage scheme. The first stage is a global preconditioner that employs multiscale basis functions to construct coarse-scale coupled systems using a Galerkin projection. This global stage is effective at damping low-frequency error modes associated with long-range coupling of the unknowns. The second stage is a local block-triangular smoothing preconditioner, which is aimed at high-frequency error modes associated with short-range coupling of the variables. Various numerical experiments are used to demonstrate the robustness of the proposed solver.

Keywords Poromechanics · Multiscale methods · Preconditioners · Iterative methods

1 Introduction

Understanding the poromechanical response of subsurface formations is essential for making predictions, quantifying the uncertainty, and assessing risk. In real-field applications, it is challenging to employ the fine-scale characterization (geometry and properties) of the subsurface system. This is largely due to the multiscale nature of the properties—e.g., permeability, mechanical moduli—and the topologic and geometric complexities of the geological structures. Here, we employ multiscale formulations and solution algorithms that are especially designed for accurate modeling of the dynamics in highly heterogeneous subsurface formations. Different up- and downscaling techniques are used in each multiscale approach to account for the connection between scales—for a review on existing multiscale methods the reader is referred to [40]. In this paper, we focus on the poroelasticity problem in heterogeneous domains.

A two-field displacement-pressure formulation based on the continuous Finite Element (FE) method—i.e. the most popular technique used in consolidation modeling, e.g. [55, 65, 73, 88]—has been traditionally used for the numerical solution of the Biot poroelasticity equations. When strong contrasts in permeability are present, discontinuous pressure interpolation may be more appropriate. Moreover, local (element-wise) mass conservation is often an essential requirement in the geoscience context—for example, in applications involving complex multiphase flow [47] or thermal convection [17].

N. Castelletto
E-mail: castelletto1@llnl.gov

S. Klevtsov ✉
E-mail: klevtsov@stanford.edu

H. Hajibeygi ✉
E-mail: H.Hajibeygi@tudelft.nl

H. A. Tchelepi ✉
E-mail: tchelepi@stanford.edu

¹Energy Resources Engineering, Stanford University, United States

²Atmospheric, Earth and Energy Division, Lawrence Livermore National Laboratory, United States

³Department of Geoscience and Engineering, Faculty of Civil Engineering and Geosciences, Delft University of Technology, Delft, The Netherlands

Hence, formulations that utilize finite elements for mechanics and finite volumes (FVs) for fluid flow are typically employed by modelers [50, 72, 78]. Motivated by the necessity of accounting for mechanical effects in applications where flow processes are of predominant importance, some authors have recently started investigating face-centered and cell-centered finite-volume methods for mechanics as well [27, 49, 66, 67]. Also, alternative approaches have been established focusing on displacement-velocity-pressure (three-field) or stress tensor-displacement-velocity-pressure (four-field) formulations, respectively—e.g., [4, 9, 10, 32, 33, 38, 42, 46, 58, 70, 71, 74, 83, 90].

Irrespective of the selected spatial discretization techniques, the solution of fully-implicit linear systems produced by any formulation cannot rely on sparse direct solvers for large-size practical applications, therefore the availability of rapidly convergent iterative methods is key. Intense research concerning the design of efficient iterative solvers has been carried out in particular for the displacement-pressure formulation of Biot’s problem. Most of the efforts have been targeting preconditioned Krylov solvers [1, 7, 8, 37, 54, 87, 89] and multigrid methods [35, 36, 60, 61]. The analysis of block preconditioners for the displacement-velocity-pressure formulation has been given increasing attention during recent years [20, 32, 83].

In this work, the focus is on the fully-implicit solution of linear systems arising from the discretization of Biot’s equations using the classic displacement-pressure formulation based on a mixed FE-FV approach. We combine multiscale methods, which were originally developed for the pressure equations and the linear momentum balance, to construct an effective preconditioner for the displacement-pressure linear system. Specifically, our approach is founded on the multiscale finite element method (MSFE) originally proposed in [41] for elliptic problems arising from composite materials and flows in porous media, and its conservative reformulation as a multiscale finite volume method (MSFV) for subsurface flow and transport developed in [44, 45].

Based on a two-grid approach, multiscale methods construct accurate coarse-scale systems using locally computed sets of base functions. Once the coarse-scale solution is obtained, it is mapped onto the original fine-scale resolution—again using the basis functions. To provide control on the accuracy of the multiscale solution to a desired level, iterative strategies may be used [39, 68], which have proved particularly useful in porous media characterized by correlated permeability fields with high contrasts [81, 85, 92]. Most of the multiscale developments have focused on fluid flow, which allowed for establishing an advanced simulation framework for flow in heterogeneous reservoirs with complex nonlinear fluid physics—e.g., [24, 25, 53, 56, 57, 64, 80, 86]. Multiscale formulations for geomechanics have appeared only recently. However, the increasing demand for accurate and efficient simulation of coupled poromechanical effects in the geoscience community provides a strong motive to develop a multiscale approach that models coupled fluid flow and geomechanical deformation. The Multiscale Finite-Element (MSFE) method has been applied to the vector partial differential equations for the elasticity problem [29]. Recent applications to linear elasticity—both as an approximate, non-iterative solver, and a preconditioner—include [14, 15, 19, 79]. Applications to consolidation of heterogeneous porous media is presented by [2, 12, 13, 26, 91].

The proposed preconditioner combines the two key ingredients of a classic two-level technique [75]: (i) construction and solution of an accurate coarse-scale system to resolve low-frequency errors in a global stage, and (ii) a fine-scale smoothing operator, which is used to rapidly damp the high-frequency error components, in a local stage. For the global stage, following an approach similar to that used in [48] for the mixed formulation of Darcy’s flow problem, we combine the multiscale basis functions used for interpolating the coarse-scale displacement and pressure fields on the fine-scale grid in a global block-diagonal multiscale operator that is used to compute the coarse (upscaled) coupled systems using a Galerkin projection. Building on the extensive research carried out in the context of block-partitioned solvers for coupled poromechanics, e.g., [7, 20, 36, 37, 87, 89], the local stage relies on a block triangular operator as the smoother.

The paper is organized as follows. In Section 2, after reviewing Biot’s poroelasticity equations, the fine-scale finite-element, finite-volume formulation is presented. In Section 3, the two-stage preconditioner for the fully-implicit solution of the algebraic linear system arising from the spatial and temporal discretization is derived in detail and analyzed. Numerical results, including a synthetic two-material heterogeneous porous medium and realistic subsurface reservoirs, are presented in Section 4. A few final remarks close the paper in Section 5.

2 Problem formulation

2.1 Governing equations

We focus on a widely used displacement-pressure formulation for linear poroelasticity assuming incompressible solid and fluid constituents. The set of governing equations for saturated single-phase flow, through a deformable medium consists of a conservation law of quasi-static linear momentum and a conservation law of mass [23, 84]. Let Ω denote the open region occupied by the porous medium. The domain boundary is decomposed as $\Gamma = \Gamma_{\mathbf{u}}^D \cup \Gamma_{\mathbf{u}}^N = \Gamma_p^D \cup \Gamma_p^N$, where $\Gamma_{\mathbf{u}}^D \cap \Gamma_{\mathbf{u}}^N = \Gamma_p^D \cap \Gamma_p^N = \emptyset$. Let \mathbf{n} and $\boldsymbol{\xi}$ denote the outer normal-vector for Γ and the position vector, respectively. The problem is time-dependent in the interval $\mathbb{I} = (0, T]$.

The solution of the quasi-static poroelastic initial boundary value problem (IBVP) are the functions $\mathbf{u}(\boldsymbol{\xi}, t)$ and $p(\boldsymbol{\xi}, t)$ that satisfy:

$$-\nabla \cdot (\mathbf{C}_{\text{dr}} : \nabla^s \mathbf{u} - p \mathbf{1}) = \mathbf{0} \quad \text{on } \Omega \times \mathbb{I} \quad (1a)$$

$$\nabla \cdot \dot{\mathbf{u}} - \nabla \cdot (\boldsymbol{\lambda} \cdot \nabla p) = s \quad \text{on } \Omega \times \mathbb{I} \quad (1b)$$

subject to the following boundary

$$\mathbf{u} = \bar{\mathbf{u}} \quad \text{on } \Gamma_{\mathbf{u}}^D \times \mathbb{I} \quad (1c)$$

$$(\mathbf{C}_{\text{dr}} : \nabla^s \mathbf{u} - p \mathbf{1}) \cdot \mathbf{n} = \bar{\mathbf{t}} \quad \text{on } \Gamma_{\mathbf{u}}^N \times \mathbb{I} \quad (1d)$$

$$p = \bar{p} \quad \text{on } \Gamma_p^D \times \mathbb{I} \quad (1e)$$

$$-(\boldsymbol{\lambda} \cdot \nabla p) \cdot \mathbf{n} = \bar{w} \quad \text{on } \Gamma_p^N \times \mathbb{I} \quad (1f)$$

and initial conditions

$$\mathbf{u}(\boldsymbol{\xi}, 0) = \mathbf{u}_0(\boldsymbol{\xi}) \quad \boldsymbol{\xi} \in \Omega \quad (1g)$$

$$p(\boldsymbol{\xi}, 0) = p_0(\boldsymbol{\xi}) \quad \boldsymbol{\xi} \in \Omega \quad (1h)$$

where \mathbf{u} and p are the displacement vector and the pore-pressure increment relative to an initial reference state; \mathbf{C}_{dr} is the drained rank-4 elasticity tensor, $\mathbf{1}$ is the rank-2 identity tensor. Moreover, $\boldsymbol{\lambda} = (\boldsymbol{\kappa}/\mu)$ is the rank-2 mobility tensor, with $\boldsymbol{\kappa}$ the intrinsic permeability tensor and μ the fluid viscosity, that is assumed constant; s is a volumetric source term; $\nabla \cdot$, ∇ and ∇^s are the divergence, the gradient and the symmetric gradient operator, respectively. The superposed dot, $(\dot{\cdot})$, denotes a derivative with respect to time t , and $\bar{\mathbf{u}}$, $\bar{\mathbf{t}}$, \bar{p} , \bar{w} are known functions. The subscript 0 is used to denote the initial state.

2.2 Discrete formulation

The discrete weak form of the poroelastic IBVP is obtained by combining a finite-element, finite volume approach for the spatial discretization with a fully-implicit backward Euler time marching scheme.

Let us introduce a conforming triangulation of the domain \mathcal{T}^h consisting of n_n nodes and n_e elements K such that $\Omega \approx \Omega^h = \bigcup_{i=1}^{n_e} K_i$. Segments of the discrete domain boundary Γ^h subject Dirichlet or a Neumann condition are denoted by $\Gamma_i^{D,h}$ and $\Gamma_i^{N,h}$, respectively, $i = \{\mathbf{u}, p\}$. The boundary of an element is denoted by ∂K and consists of interfaces—i.e., edges or faces—that are shared by at most two elements. Every interface δ is assigned with a unit normal vector \mathbf{n}_δ that determines its global orientation. For an internal interface δ shared by elements K_1 and K_2 , \mathbf{n}_δ points outside of K_1 into K_2 , namely in the direction of increasing global element indices. For a boundary interface \mathbf{n}_δ is oriented outside of Ω^h . The spatial discretization relies on the following approximation spaces for the displacement and pressure field, respectively, associated with the computational mesh

$$\mathcal{U}^h := \{\mathbf{v} \mid \mathbf{v} \in [C^0(\Omega)]^{n_{\text{sd}}}, \mathbf{v} = \bar{\mathbf{u}} \text{ on } \Gamma_{\mathbf{u}}^D, \mathbf{v}|_K \in [\mathbb{Q}_1(K)]^{n_{\text{sd}}} \forall K \in \mathcal{T}^h\}, \quad (2)$$

$$\mathcal{P}^h := \{q \mid q \in L^2(\Omega), q|_K \in \mathbb{P}_0(K) \forall K \in \mathcal{T}^h\}, \quad (3)$$

with $C^0(\Omega)$ and $L^2(\Omega)$ the space of continuous and square Lebesgue-integrable functions on Ω , and n_{sd} the spatial dimension of the problem. Precisely, on each K a piecewise bilinear ($n_{\text{sd}} = 2$) or trilinear ($n_{\text{sd}} = 3$) interpolation is used for the displacement vector, whereas the approximate pressure is piecewise constant. An appropriate approximation for inter-element Darcy's flux is also needed to complete the formulation. Let $F^{K,\delta}$ denote the approximation to the following flux through interface $\delta \in \partial K$

$$F^{K,\delta}(p^h, \bar{p}) \approx \int_{\delta} (\boldsymbol{\lambda} \cdot \nabla p) \cdot \mathbf{n}_K \, dA, \quad (4)$$

with \mathbf{n}_K the unit outward normal vector to ∂K . Flux $F^{K,\delta}$ is expressed based on a suitable functional dependence on element pressure $p^h \in \mathcal{P}^h$ and prescribed boundary pressure \bar{p} . Local conservation constraints the flux through an internal interface δ shared by elements K_1 and K_2 to satisfy the relationship

$$F^{K_1, \delta}(p^h, \bar{p}) + F^{K_2, \delta}(p^h, \bar{p}) = 0. \quad (5)$$

We use a linear two-point flux approximation (TPFA) scheme [3], which is the industry standard for reservoir simulation because of its robustness and ease of implementation. Because the problem is linear, $F^{K, \delta}$ can be written as a sum of two terms

$$F^{K, \delta}(p^h, \bar{p}) = \hat{F}^{K, \delta}(p^h) + \bar{F}^{K, \delta}(\bar{p}), \quad (6)$$

to emphasize the contribution to the flux that depends on p^h and \bar{p} , respectively. Note that $\bar{F}^{K, \delta}$ is nonzero only for non homogeneous prescribed boundary pressure values. Due to the lack of consistency of the scheme [28, 30], we recognize that a linear TPFA approach may lead to inaccurate results for highly distorted grid or full-permeability tensors. In such cases more sophisticated discretization methods like multipoint and/or nonlinear schemes are needed. For details on recent developments for heterogeneous anisotropic diffusion problems see [28, 77, 82] and references therein. Convergence results of the mixed FEM-FV formulation for the Biot problem were reported in [21].

Time integration is carried out by partitioning the time interval \mathbb{I} into $n_{\Delta t}$ subintervals $\mathbb{I}_n = (t_{n-1}, t_n]$, $n = 1, \dots, n_{\Delta t}$, where $\Delta t_n = (t_n - t_{n-1})$. The displacement time derivative in (1b), which accounts for the change in fluid storage volume due to mechanical dilation of the pore space, is discretized using a simple incremental ratio. The remaining terms are approximated at time t_n .

Given $\mathbf{u}^h, \mathbf{v}^h \in \mathcal{U}^h$ and $p^h, q^h \in \mathcal{P}^h$, it is convenient to define for each $K \in \mathcal{T}^h$ the following bilinear forms

$$a_K(\mathbf{v}^h, \mathbf{u}^h) := \int_K \nabla^s \mathbf{v}^h : \mathbf{C}_{\text{dr}} : \nabla^s \mathbf{u}^h \, dV, \quad (7a)$$

$$b_K(\mathbf{v}^h, p^h) := \int_K \nabla \cdot \mathbf{v}^h p^h \, dV, \quad (7b)$$

$$c_K(q^h, p^h) := -q^h|_K \sum_{\delta \in \partial K \setminus \partial K_p^N} \hat{F}^{K, \delta}(p^h), \quad (7c)$$

and functionals

$$f_K(\mathbf{v}^h) := \int_{\partial K_{\mathbf{u}}^N} \mathbf{v}^h \cdot \bar{\mathbf{t}} \, dA, \quad (7d)$$

$$g_K(q^h) := q^h|_K \sum_{\delta \in \partial K \setminus \partial K_p^N} \bar{F}^{K, \delta}(\bar{p}) + \int_K q^h s \, dV - \int_{\partial K_p^N} q^h \bar{w} \, dA, \quad (7e)$$

where $\partial K_{\mathbf{u}}^N = \partial K \cap \Gamma_{\mathbf{u}}^{N, h}$ and $\partial K_p^N = \partial K \cap \Gamma_p^{N, h}$. The above forms and functionals can be defined on Ω as:

$$a(\mathbf{v}^h, \mathbf{u}^h) := \sum_{K \in \mathcal{T}^h} a_K(\mathbf{v}^h, \mathbf{u}^h), \quad (8a)$$

$$b(\mathbf{v}^h, p^h) := \sum_{K \in \mathcal{T}^h} b_K(\mathbf{v}^h, p^h), \quad (8b)$$

$$c(q^h, p^h) := \sum_{K \in \mathcal{T}^h} c_K(q^h, p^h), \quad (8c)$$

$$f(\mathbf{v}^h) := \sum_{K \in \mathcal{T}^h} f_K(\mathbf{v}^h), \quad (8d)$$

$$g(q^h) := \sum_{K \in \mathcal{T}^h} g_K(q^h). \quad (8e)$$

Finally, the mesh-dependent fully discrete weak form of Biot's poroelasticity equations can be stated as follows [31, 43]: given \mathbf{u}_0 , and p_0 , find $\{\mathbf{u}_n^h, p_n^h\} \in \mathcal{U}^h \times \mathcal{P}^h$ such that for $n = \{1, \dots, n_{\Delta t}\}$

$$a(\mathbf{v}^h, \mathbf{u}_n^h) - b(\mathbf{v}^h, p_n^h) = f_n(\mathbf{v}^h) \quad \forall \mathbf{v}^h \in \mathcal{U}_0^h, \quad (9a)$$

$$b\left(\frac{\mathbf{u}_n^h - \mathbf{u}_{n-1}^h}{\Delta t_n}, q^h\right) + c(q^h, p_n^h) = g_n(q^h) \quad \forall q^h \in \mathcal{P}^h, \quad (9b)$$

with \mathcal{U}_0^h the subspace of the trial functions belonging to \mathcal{U}^h satisfying homogeneous boundary displacement on $\Gamma_{\mathbf{u}}^{D,h}$.

2.3 Matrix form

Problems such as (9) produce a sequence of 2×2 block linear systems of the form

$$\mathbf{A}_n \mathbf{x}_n = \mathbf{b}_n, \quad n = \{1, \dots, n_{\Delta t}\} \quad (10)$$

with

$$\mathbf{A}_n = \begin{bmatrix} A & -B \\ B^T & \Delta t_n C \end{bmatrix}, \quad \mathbf{x}_n = \begin{Bmatrix} \mathbf{d}_n \\ \mathbf{p}_n \end{Bmatrix}, \quad \mathbf{b}_n = \begin{Bmatrix} \mathbf{f}_n \\ \Delta t_n \mathbf{g}_n - B^T \mathbf{d}_{n-1} \end{Bmatrix}. \quad (11)$$

Vectors $\mathbf{d}_n \in \mathbb{R}^{n_u}$ and $\mathbf{p}_n \in \mathbb{R}^{n_p}$ collect the n_u nodal displacement and n_p cell-centered pressure degrees of freedom (DOFs), respectively, with $n_u = n_{sd} n_n$ and $n_p = n_e$, that are used to approximate \mathbf{u}_n^h and p_n^h as

$$\mathbf{u}_n^h(\boldsymbol{\xi}) = N_{\mathbf{u}}(\boldsymbol{\xi}) \mathbf{d}_n, \quad (12a)$$

$$p_n^h(\boldsymbol{\xi}) = N_p(\boldsymbol{\xi}) \mathbf{p}_n, \quad (12b)$$

where columns of matrices $N_{\mathbf{u}} \in \mathbb{R}^{n_{sd} \times n_u}$ and $N_p \in \mathbb{R}^{1 \times n_p}$ contain the basis functions for spaces \mathcal{U}^h and \mathcal{P}^h . Since the displacement Dirichlet boundary conditions (1c) are not used in the definition (12a), matrices A and B are generated ignoring the essential boundary conditions, which are then prescribed in a strong sense. Prescribed boundary pressure values (1e) are weakly imposed in this formulation. The matrix A is the stiffness matrix of a ‘pure’ mechanics problem. Because we assume a linear elastic constitutive law in this work, A is symmetric positive definite (SPD). The matrix C represents the standard Darcy-flow problem, and it is also SPD given the assumptions of fluid incompressibility and constant viscosity—note that for compressible fluid flow C is in general non-symmetric and indefinite [3]. The off-diagonal matrix B is the stress-flow coupling matrix.

3 Numerical solution algorithm

Solving the sequence of fully-implicit linear systems (10) represents the most expensive computation kernel in coupled poromechanics simulation. As the problem size (number of computational cells) increases, global iterative solution strategies are the method of choice—typically non-symmetric Krylov solvers, such as the generalized minimal residual (GMRES) method [76]. Because of the severe ill-conditioning of \mathbf{A}_n , preconditioning is essential to solve such systems efficiently. The design of a robust and efficient preconditioner is based on a trade-off between two competing objectives [5]: (i) reducing the number of iterations needed by the preconditioned solver to achieve convergence (robustness), and (ii) limiting the time required to construct and apply the preconditioner (efficiency). In this work, we devise a two-stage (or two-level) preconditioning strategy for (10) that combines a global (\mathbf{M}_G^{-1}) and a local preconditioner (\mathbf{M}_L^{-1}). In particular, \mathbf{M}_G^{-1} is based on multiscale methods aimed at damping low-frequency error modes associated with long-range coupling of the unknowns. The second stage, \mathbf{M}_L^{-1} , complements \mathbf{M}_G^{-1} by tackling high-frequency error modes associated with short-range coupling of the variables. The overall preconditioner is then used in conjunction with GMRES using its right-preconditioned version.

3.1 Global multiscale preconditioner (\mathbf{M}_G^{-1})

The original idea of multiscale finite-element (MSFE) and finite-volume (MSFV) methods is to provide approximate solutions of high-resolution fine-scale problems at low computational cost. Based on a two-grid approach, these methods compute sets of basis functions that are used to construct coarse-scale global operators that are significantly less expensive to solve than the original fine-scale system. The solution of the coarse-scale problem is mapped to the fine-scale using the basis functions. Let \mathcal{T}^H be the coarse grid superimposed on the given fine-scale grid \mathcal{T}^h , where the hydro-mechanical properties

are provided. A coarse element in \mathcal{T}^H is an aggregate of fine-scale elements. In addition to \mathcal{T}^H , the MSFV method requires the definition of an overlapping dual-coarse grid. Once coarse grids are defined, basis functions are computed independently solving local problems subject to Dirichlet boundary conditions derived by a localization assumption [41, 44]. Each basis function is associated with a coarse scale DOF. In particular, we denote by $n_{\mathbf{u}}^H = n_{sd}n_n^H$ and $n_p^H = n_e^H$ the number of coarse scale displacement and pressure DOFs, with n_n^H and n_e^H the number of nodes and elements in \mathcal{T}^H .

In this work independent sets of basis functions are derived for the displacement and the pressure field, respectively, as suggested in [18]. The multiscale approximation to the fine-scale fields (12) is expressed as:

$$\mathbf{u}_n^h(\boldsymbol{\xi}) \approx \mathbf{u}_n^{h,MS}(\boldsymbol{\xi}) = N_{\mathbf{u}}^H(\boldsymbol{\xi})\mathbf{d}_n^H = \underbrace{N_{\mathbf{u}}(\boldsymbol{\xi})P_{\mathbf{u}}}_{=N_{\mathbf{u}}^H(\boldsymbol{\xi})}\mathbf{d}_n^H, \quad (13a)$$

$$p_n^h(\boldsymbol{\xi}) \approx p_n^{h,MS}(\boldsymbol{\xi}) = N_p^H(\boldsymbol{\xi})p_n^H = \underbrace{N_p(\boldsymbol{\xi})P_p}_{=N_p^H(\boldsymbol{\xi})}p_n^H, \quad (13b)$$

where $\mathbf{d}_n^H \in \mathbb{R}^{n_{\mathbf{u}}^H}$, $\mathbf{p}_n^H \in \mathbb{R}^{n_p^H}$, $N_{\mathbf{u}}^H \in \mathbb{R}^{n_{sd} \times n_n^H}$, and $N_p^H \in \mathbb{R}^{1 \times n_p^H}$ are the multiscale counterparts relative to the coarse grid \mathcal{T}^H of \mathbf{d}_n , \mathbf{p}_n , $N_{\mathbf{u}}$ and N_p . Displacement coarse scale basis functions are computed solving local linear momentum balance problems assuming drained conditions [14, 15, 19], while pressure multiscale basis functions are constructed computing local solutions to incompressible flow problems [44]. Note that in (13) matrices containing the multiscale basis functions are expressed as linear combination of the fine scale basis functions contained in $N_{\mathbf{u}}$ and N_p , with the discrete values at fine scale nodes and elements stored in the two sparse linear operators $P_{\mathbf{u}} \in \mathbb{R}^{n_{\mathbf{u}} \times n_n^H}$ and $P_p \in \mathbb{R}^{n_p \times n_p^H}$, respectively. The basis functions are computed in a preprocessing phase and remain constant during the entire time-dependent simulation. From (13) it is clear that $P_{\mathbf{u}}$ and P_p serve as prolongation (interpolation) operators transferring vectors associated with the coarse grid \mathcal{T}^H to the fine grid \mathcal{T}^h , i.e.

$$P_{\mathbf{u}} : \mathbb{R}^{n_{\mathbf{u}}^H} \rightarrow \mathbb{R}^{n_{\mathbf{u}}}, \mathbf{d}^H \mapsto \mathbf{d}^{MS} = P_{\mathbf{u}}\mathbf{d}^H, \quad (14a)$$

$$P_p : \mathbb{R}^{n_p^H} \rightarrow \mathbb{R}^{n_p}, \mathbf{p}^H \mapsto \mathbf{p}^{MS} = P_p\mathbf{p}^H. \quad (14b)$$

The multiscale formulation allows for approximating the fine-scale solution of the linear system (10) as the expansion of a coarse-scale solution. If $P_{\mathbf{u}}$ and P_p are combined together in a global separate displacement-pressure block diagonal prolongation operator \mathbf{P} , we have:

$$\mathbf{x}_n \approx \mathbf{x}_n^{MS} = \begin{Bmatrix} \mathbf{d}_n^{MS} \\ \mathbf{p}_n^{MS} \end{Bmatrix} = \begin{bmatrix} P_{\mathbf{u}} \\ P_p \end{bmatrix} \begin{Bmatrix} \mathbf{d}_n^H \\ \mathbf{p}_n^H \end{Bmatrix} = \mathbf{P}\mathbf{x}_n^H. \quad (15)$$

Since \mathbf{P} is assembled in a setup stage, it is sufficient to calculate $\mathbf{x}_n^H \in \mathbb{R}^{n_{\mathbf{u}}^H + n_p^H}$ to obtain the fine scale approximation $\mathbf{x}_n^{MS} \in \mathbb{R}^{n_{\mathbf{u}} + n_p}$. To compute \mathbf{x}_n^H , first \mathbf{x}_n is replaced by \mathbf{x}_n^{MS} in (10), then the resulting residual, i.e. $\mathbf{r}_n^{MS} = (\mathbf{b}_n - \mathbf{A}\mathbf{P}\mathbf{x}_n^H)$, is orthogonalized against $(n_{\mathbf{u}}^H + n_p^H)$ vectors in $\mathbb{R}^{n_{\mathbf{u}} + n_p}$, which form the rows of the operator \mathbf{R} . Hence, \mathbf{x}_n^H is the solution to the linear system

$$\mathbf{A}_n^H \mathbf{x}_n^H = \mathbf{b}_n^H, \quad (16)$$

with $\mathbf{A}_n^H = \mathbf{R}\mathbf{A}_n\mathbf{P}$, and $\mathbf{b}_n^H = \mathbf{R}\mathbf{b}_n$. We refer to \mathbf{R} as the restriction operator that is used to map vectors from fine- to coarse scale. Different options may be considered for \mathbf{R} . In this work, we focus on a Galerkin orthogonalization approach, i.e. the one used in the MSFE method, therefore $\mathbf{R} = \mathbf{P}^T$. We observe that in the MSFV method a Petrov-Galerkin strategy is used for the pressure restriction sub-operator [44].

The multiscale approximate solution \mathbf{x}_n^{MS} to (10) can be formally written as:

$$\mathbf{x}_n^{MS} = \mathbf{P}\mathbf{x}_n^H = \mathbf{P}(\mathbf{A}_n^H)^{-1}\mathbf{b}_n^H = \mathbf{P}(\mathbf{P}^T\mathbf{A}_n\mathbf{P})^{-1}\mathbf{P}^T\mathbf{b}_n, \quad (17)$$

which provides the expression of the global multiscale preconditioner \mathbf{M}_G^{-1} , i.e.,

$$\mathbf{M}_G^{-1} = \mathbf{P}(\mathbf{P}^T\mathbf{A}_n\mathbf{P})^{-1}\mathbf{P}^T. \quad (18)$$

Efficient solution of the coarse-scale system is key for the performance of \mathbf{M}_G^{-1} . As opposed to two-grid methods in the multigrid context, the multiscale basis functions, combined with proper coarsening ratios, are capable of accurately capturing fine-scale features at the coarse level, thus making the two-level strategy a competitive option. In our implementation, the coarse system is solved using a direct solver. Having the multiscale preconditioner rank $(n_u^H + n_p^H) < (n_u + n_p)$, the use of \mathbf{M}_G^{-1} alone would not allow to expand the Krylov subspace beyond $(n_u^H + n_p^H)$. Indeed, \mathbf{M}_G^{-1} is responsible for tackling low-frequency error components only and must be complemented by a local smoothing preconditioner removing the high frequency errors.

Remark 1 The appealing feature of the MSFV method (Petrov-Galerkin orthogonalization) is that it warrants mass conservation on the primal coarse grid [44]. This is also the case when MSFV is used as an iterative solver [59]. However, the iterative performance of MSFV is typically overcome by an iterative MSFE-based approach (Galerkin orthogonalization)—see, for instance, [85]. If a relatively loose tolerance is used to control the convergence, the lack of mass conservation in MSFE can be rectified by applying MSFV once to the residual in a final step [85].

3.2 Local block-triangular smoothing preconditioner (\mathbf{M}_L^{-1})

When dealing with linear systems arising from the discretization of coupled PDEs, an often used approach is to design preconditioners starting from a block LDU-factorization of the system matrix [6, 11], namely,

$$\mathbf{A}_n = \mathbf{LDU} = \begin{bmatrix} I_u & & \\ B^T A^{-1} & I_p & \\ & & \end{bmatrix} \begin{bmatrix} A & \\ & S \end{bmatrix} \begin{bmatrix} I_u & -A^{-1}B \\ & I_p \end{bmatrix}, \quad (19)$$

where I_u and I_p are identity operators in \mathbb{R}^{n_u} and \mathbb{R}^{n_p} , respectively, and $S = (\Delta t_n C + B^T A^{-1} B)$ is the Schur complement of A in \mathbf{A}_n . Using a block-upper triangular approximation for the system matrix, i.e. $\mathbf{A}_n \approx \mathbf{DU}$, we consider the following operator as a local preconditioner for \mathbf{A}_n :

$$\mathbf{M}_L^{-1} = \begin{bmatrix} \tilde{A} & -B \\ & \tilde{S} \end{bmatrix}^{-1} = \begin{bmatrix} \tilde{A}^{-1} & \\ & I_p \end{bmatrix} \begin{bmatrix} I_u & B \\ & I_p \end{bmatrix} \begin{bmatrix} I_u & \\ & \tilde{S}^{-1} \end{bmatrix}, \quad (20)$$

where \tilde{A}^{-1} and \tilde{S}^{-1} denote cheap local preconditioners for A and S —i.e., inexact solvers for linear system involving A and S . Several software packages offer off-the-shelf local preconditioners that can be readily used for the mechanical subproblem and also for the Schur complement, provided that a good sparse approximation for S —which is quite dense given the term A^{-1} —is available. Here, we follow the well-established approach that relies on the so-called *fixed-stress* solution scheme of two-way coupled poromechanics. Originally introduced as an operator split method in the context of unconditionally stable sequential methods for flow and geomechanics [34, 50, 51, 63, 78], the method was later reinterpreted as a block-preconditioned Richardson iteration [89]. In essence, the fixed-stress is the argument supporting a physically-based approximation to the Schur complement that replaces the triple product $B^T A^{-1} B$ in S with a pressure space mass matrix M_p (possibly lumped) scaled by a weighting factor, which depends element-wise on the bulk modulus of the medium and Biot's coefficient [21, 89], i.e. $S \approx S_{FS} = \Delta t_n C + M_p$ with $M_p \approx B^T A^{-1} B$. Note that in the present work, the Biot coefficient is always equal to unity, since incompressible grains are assumed. Here, given the piecewise constant interpolation used for the pressure, M_p is diagonal. Fully algebraic generalizations of the fixed-stress approximation based on probing [52] and element-by-element [20] techniques have also been proposed.

Remark 2 Block triangular operators have proved to be effective, scalable preconditioners for Krylov subspace methods applied to linear systems arising in poromechanics based on a wide range of formulations. When used as preconditioners, the effort is on designing good sparse Schur complement approximations. Later, the action of subproblem and Schur complement inverses are typically applied using high quality preconditioners based on multigrid, domain decomposition or approximate inverses methods. Here, we pursue a different approach and propose the use of a block triangular operator as smoothing operator that complements the global multiscale preconditioner. The objective is to keep subproblem preconditioners \tilde{A}^{-1} and \tilde{S}^{-1} as cheap as possible—typically relaxation preconditioners (e.g. Jacobi, Gauss-Seidel) or incomplete factorizations—while an accurate solution is computed for the (much smaller) coarse system.

3.3 Multiscale-based two-stage preconditioner (\mathbf{M}_n^{-1})

The overall two-stage preconditioner is obtained combining \mathbf{M}_G^{-1} and \mathbf{M}_L^{-1} in a multiplicative fashion. Given a matrix K in $\mathbb{R}^{n \times n}$, a general form for a multiplicative multi-stage preconditioner \tilde{K}^{-1} can be written as [16]

$$\tilde{K}^{-1} = \tilde{K}_1^{-1} + \sum_{i=2}^{n_\ell} \tilde{K}_i^{-1} \prod_{j=1}^{i-1} [I - K \tilde{K}_j^{-1}] \quad (21)$$

with n_ℓ the number of stages, \tilde{K}_k^{-1} , $k \in \{1, \dots, n_\ell\}$, the n_ℓ preconditioners for K , and I the identity matrix in $\mathbb{R}^{n \times n}$. The multiscale-based two-stage preconditioner \mathbf{M}_n^{-1} is obtained by specializing equation (21) with \mathbf{M}_G^{-1} and \mathbf{M}_L^{-1} serving as first- and second-stage preconditioner, respectively. In operator form, the action of \mathbf{M}_n^{-1} on a vector $\mathbf{w} \in \mathbb{R}^{n_u + n_p}$ can be summarized as follows:

$$\mathbf{M}_n^{-1} : \mathbb{R}^{n_u + n_p} \rightarrow \mathbb{R}^{n_u + n_p}, \mathbf{w} \mapsto \mathbf{z} = [\mathbf{M}_G^{-1} + \mathbf{M}_L^{-1} (\mathbf{I} - \mathbf{A}_n \mathbf{M}_G^{-1})] \mathbf{w}, \quad (22)$$

with \mathbf{I} the identity matrix in $\mathbb{R}^{(n_u + n_p) \times (n_u + n_p)}$.

We focus on a linear poroelastic model problem; therefore, blocks in system matrix \mathbf{A}_n do not depend on the solution vector \mathbf{x}_n . The time step size is the only term that may change between consecutive system solves. Hence, the construction of the two-stage preconditioner may be split in two phases. First, the preconditioner components that can be reused throughout the transient simulation are computed in a setup phase. Then, the remaining tasks required for the computation of \mathbf{M}_n^{-1} are accomplished during an update phase, which has to be performed whenever Δt_n varies. The two phases are summarized in Algorithms 1 and 2. Overall, the preconditioner requires one solve for \mathbf{A}_n^H , one solve for \hat{A} , one solve for \hat{S} , and four matrix-vector products with \mathbf{P}^T , \mathbf{P} , \mathbf{A}_n , and B , respectively. The sequence of operations needed to apply \mathbf{M}_n^{-1} are given in Algorithms 3 to 5.

Remark 3 The second-stage local preconditioner, namely steps 2 to 5 in Algorithm 3, can be regarded as the first iteration of the following relaxation scheme:

$$\mathbf{z}_k = \mathbf{z}_{k-1} + \omega \mathbf{M}_L^{-1} \mathbf{r}_{k-1} \quad (23)$$

with $k = \{1, 2, \dots\}$ the iteration counter, ω a scalar relaxation parameter (equal to 1 in Algorithm 3), and $\mathbf{r}_{k-1} = (\mathbf{w} - \mathbf{A}_n \mathbf{z}_{k-1})$ the residual vector. The preconditioner performance can be improved by performing several iterations of the relaxation scheme (23) at each preconditioning step.

The robustness and efficiency of \mathbf{M}_n^{-1} depend on the ability of the global and local stages to deal with the full error spectrum. The proposed operator \mathbf{M}_n^{-1} is used to precondition system (10) from the right, which is the typical strategy when residual minimization methods, such as GMRES, are used. Assuming that the preconditioned matrix can be diagonalized, the convergence behavior of GMRES is controlled by the spectral properties of the preconditioned matrix, including condition number as well as the distribution of the eigenvalues [75]. However, computational experience shows that a preconditioned matrix with clustered eigenvalues away from 0 usually denote a favorable condition for fast convergence. It is therefore useful to gain some insight on the eigenvalues on the preconditioned matrix for a better assessment of the preconditioning operator. Proceeding as in [69], the right preconditioned system matrix can be rewritten as

$$\mathbf{A}_n \mathbf{M}_n^{-1} = \mathbf{A}_n \mathbf{M}_G^{-1} + \mathbf{A}_n \mathbf{M}_L^{-1} - \mathbf{A}_n \mathbf{M}_L^{-1} \mathbf{A}_n \mathbf{M}_G^{-1} = \mathbf{I} - \mathbf{R}_L \mathbf{R}_G, \quad (24)$$

where $\mathbf{R}_L = (\mathbf{I} - \mathbf{A}_n \mathbf{M}_L^{-1})$ and $\mathbf{R}_G = \mathbf{I} - \mathbf{A}_n \mathbf{M}_G^{-1}$ are residual matrices that quantify the quality of the local and global preconditioners in approximating the action of \mathbf{A}_n^{-1} . Using (24), the right-preconditioned matrix eigenvalues are expressed as

$$\lambda(\mathbf{A}_n \mathbf{M}_n^{-1}) = 1 - \lambda(\mathbf{R}_L \mathbf{R}_G). \quad (25)$$

Hence, we can bound their distance from the unity as follows:

$$|\lambda(\mathbf{A}_n \mathbf{M}_n^{-1}) - 1| = |\lambda(\mathbf{R}_L \mathbf{R}_G)| \leq \|\mathbf{R}_L\| \|\mathbf{R}_G\|, \quad (26)$$

where $\|\cdot\|$ denotes any compatible matrix norm. Given that $\text{rank}(\mathbf{A}_n \mathbf{M}_G^{-1}) = \text{rank}(\mathbf{M}_G^{-1}) = (n_u^H + n_p^H) < (n_u + n_p)$, the eigenvalues of \mathbf{R}_G can be expressed as

$$|\lambda(\mathbf{R}_G)| = \begin{cases} 1 & \text{with multiplicity } (n_u + n_p) - (n_u^H + n_p^H), \\ \varepsilon_i & i = 1, \dots, (n_u^H + n_p^H). \end{cases} \quad (27)$$

Assuming that the matrix \mathbf{M}_G^{-1} is a good (low-rank) approximation of the inverse of the fine scale matrix, nonzero eigenvalues of $\mathbf{A}_n \mathbf{M}_G^{-1}$ are expected to be close to 1; therefore, $\varepsilon_i \approx 0$. If this holds true, $\|\mathbf{R}_G\| = 1$, and so (26) becomes

$$|\lambda(\mathbf{A}_n \mathbf{M}_n^{-1}) - 1| \leq \|\mathbf{R}_L\|. \quad (28)$$

To conclude, Eq. (28) tells us that the spectral properties of $\mathbf{A}_n \mathbf{M}_n^{-1}$ are not worse than $\mathbf{A}_n \mathbf{M}_L^{-1}$.

Algorithm 1 Preconditioner computation: Setup phase

- 1: Compute \mathbf{P}
 - 2: Compute \tilde{A}^{-1} as a local preconditioner of A
 - 3: Compute M_p
-

Algorithm 2 Preconditioner computation: Update phase

- 1: $\mathbf{A}_n^H = \mathbf{P}^T \mathbf{A}_n \mathbf{P}$
 - 2: Factorize $\mathbf{A}_n^H = \mathbf{L}_{\mathbf{A}_n^H} \mathbf{U}_{\mathbf{A}_n^H}$ with a direct solver
 - 3: $S_{FS} = \Delta t_n C + M_p$
 - 4: Compute \tilde{S}^{-1} as a local preconditioner of S_{FS}
-

Algorithm 3 Application of preconditioner \mathbf{M}_n^{-1}

Require: \mathbf{w}

Ensure: $\mathbf{z} = \mathbf{M}_n^{-1} \mathbf{w}$

- 1: Apply \mathbf{M}_G^{-1} to \mathbf{w} to get \mathbf{z}_0
 - 2: $\mathbf{r}_0 = \mathbf{A}_n \mathbf{z}_0$
 - 3: $\mathbf{r}_0 \leftarrow \mathbf{w} - \mathbf{r}_0$
 - 4: Apply \mathbf{M}_L^{-1} to \mathbf{r}_0 to get \mathbf{z}
 - 5: $\mathbf{z} \leftarrow \mathbf{z}_0 + \mathbf{z}$
-

Algorithm 4 Application of preconditioner \mathbf{M}_G^{-1}

Require: \mathbf{w}

Ensure: $\mathbf{z} = \mathbf{M}_G^{-1} \mathbf{w}$

- 1: $\mathbf{w}^H = \mathbf{P}^T \mathbf{w}$
 - 2: Apply $\mathbf{L}_{\mathbf{A}_n^H}^{-1}$ to \mathbf{w}^H to get \mathbf{z}^H
 - 3: Apply $\mathbf{U}_{\mathbf{A}_n^H}^{-1}$ to \mathbf{z}^H to get \mathbf{w}^H
 - 4: $\mathbf{z} = \mathbf{P} \mathbf{w}^H$
-

Algorithm 5 Application of preconditioner \mathbf{M}_L^{-1}

Require: $\mathbf{w} = \{\mathbf{w}_u^T, \mathbf{w}_p^T\}^T$
Ensure: $\mathbf{z} = \{\mathbf{z}_u^T, \mathbf{z}_p^T\}^T = \mathbf{M}_L^{-1} \mathbf{w}$
1: Apply \tilde{S}^{-1} to \mathbf{w}_p to get \mathbf{z}_p
2: $\mathbf{y} = \mathbf{B}\mathbf{z}_p$
3: $\mathbf{y} \leftarrow \mathbf{w}_u + \mathbf{y}$
4: Apply \tilde{A}^{-1} to \mathbf{y} to get \mathbf{z}_u

4 Numerical results

Two sets of numerical experiments are presented. The first set considers a synthetic two-material heterogeneous porous medium [12]. This first set is intended to evaluate the performance of the proposed preconditioner in a sequence of refined domains for different types of mesh and stiffness contrast. Then, the robustness of the two-stage method is assessed considering flow in a heterogeneous deforming synthetic reservoir.

In all the test cases, the inverse of the coarse-scale system is always applied by means of a direct solve in the global preconditioning stage. That is, the factorization $\mathbf{A}_n^H = \mathbf{L}_{A_n^H} \mathbf{U}_{A_n^H}$ is computed and followed by a forward/backward substitution. In the local preconditioning stage, incomplete Cholesky (IC) factorizations are used as local preconditioners for both the stiffness matrix and Schur complement. Thus, we have $\tilde{A}^{-1} = \tilde{L}_A^{-T} \tilde{L}_A^{-1}$ and $\tilde{S}^{-1} = \tilde{L}_S^{-T} \tilde{L}_S^{-1}$. The zero-fill in variant (IC(0))—i.e., $\tilde{A}^{-1} = A_{\text{IC}(0)}^{-1}$ and $\tilde{S}^{-1} = S_{\text{FS,IC}(0)}^{-1}$ —is always selected as default option [75]. If a breakdown occurs in the computation of $A_{\text{IC}(0)}$ because zero, or negative, pivots are encountered, we switch to the variant with threshold dropping (ICT)—i.e., $\tilde{A}^{-1} = A_{\text{ICT}(\tau_A)}^{-1}$, with τ_A the desired dropping tolerance [75]. Note that the TPFA formulation ensures that C is a SPD M -matrix and so is S_{FS} , hence the Cholesky decomposition $S_{\text{FS,IC}(0)}$ is guaranteed to be stable [62]. However, for highly heterogeneous permeability fields it proves beneficial to employ the ICT variant $S_{\text{FS,ICT}(\tau_S)}$ for the Schur complement.

In all tests, a simple block-row scaling is introduced to warrant that mechanics and flow discrete equations have comparable magnitude prior to the solution stage. Precisely, the coefficient $\alpha = \Delta t_n \frac{\|C\|_F}{\|A\|_F}$ is introduced to scale the mechanics equations, with $\|\cdot\|_F$ denoting the Frobenius norm of a matrix. For every linear solve, the null vector is always chosen as the initial guess $\mathbf{x}^{(0)}$. The stopping criterion is based on the reduction of the Euclidean norm of the iterative residual $\mathbf{r}^{(k)}$ below a specified tolerance τ , i.e., $\|\mathbf{r}^{(k)}\|_2 \leq \tau \|\mathbf{r}^{(0)}\|_2$, with k the iteration number. The numerical tests discussed in this section always use $\tau = 1 \times 10^{-6}$. The computational performance is evaluated in terms of average iteration count n_{iter} per timestep required by right preconditioned GMRES to converge to the desired accuracy. Wall clock time for the preconditioner computation (T_p) and average wall clock time for the solver to converge (\bar{T}_s) are also provided, with the average total time denoted by $\bar{T}_t = T_p + \bar{T}_s$. The following densities for the global

$$\rho_G = \frac{2 \times \text{nnz}(\mathbf{P}) + \text{nnz}(\mathbf{L}_{A_n^H}) + \text{nnz}(\mathbf{U}_{A_n^H})}{\text{nnz}(\mathbf{A}_n)} \quad (29a)$$

and the local preconditioner

$$\rho_L = \frac{2 \times \text{nnz}(\tilde{L}_A) + 2 \times \text{nnz}(\tilde{L}_S) + \text{nnz}(B)}{\text{nnz}(\mathbf{A}_n)} \quad (29b)$$

are also reported, where nnz is the function returning the number of nonzero matrix elements. The density of the overall preconditioner is given by $\rho_t = (1 + \rho_G + \rho_L)$. All the numerical experiments were carried out using Matlab on an Intel(R) Core(TM) i7-6560U processor at 2.20GHz with 16-GB of memory.

Test 1: Synthetic two-material heterogeneous porous medium

The first synthetic example, denoted as Test 1, focuses on a two-material heterogeneous problem. It makes use of the same simulation setup defined in [12]. We use the unit square as the domain, i.e. $L = W = 1$ m (Fig. 2). At time $t = 0$ we have $\mathbf{u} = \mathbf{0}$ and $p = 0$ everywhere. The domain is subject to a roller boundary condition over the left ($\xi_1 = 0$) and bottom ($\xi_2 = 0$) boundaries while the right ($\xi_1 = L$) and top ($\xi_2 = W$) boundaries are traction free. As to the flow, left and right boundaries are impervious, a constant overpressure $\bar{p} = 1$ Pa is prescribed at the top boundary, and the bottom boundary is kept at the initial condition. The domain consists of two materials as shown in Fig. 2. The poromechanical parameters are provided in Table 1.

Table 1: Test 1: simulation parameters. Fluid viscosity has a constant value $\mu = 1 \times 10^{-3}$ Pa·s.

Symbol	Quantity	Material 1	Material 2		Unit
			Test 1a	Test 1b	
E	Young's modulus	1×10^1	1×10^0	1×10^{-3}	[Pa]
ν	Poisson's ratio	0.25	0.25	0.25	[-]
κ	isotropic permeability	1×10^{-3}	1×10^0	1×10^0	[m ²]

Table 2: Test 1: Size and numbers of non-zero elements in the system matrix blocks as a function of mesh refinement level (ℓ). The total number of fine scale DOFs is $n_t = n_{\mathbf{u}} + n_p$.

ℓ	n_e	n_t	$n_{\mathbf{u}}$	n_p	$\text{nnz}(A)$	$\text{nnz}(B)$	$\text{nnz}(C)$
0	100×100	30,402	20,402	10,000	362,404	80,000	49,600
1	200×200	120,802	80,802	40,000	1,444,804	320,000	199,200
2	400×400	481,602	321,602	160,000	5,769,604	1,280,000	798,400
3	800×800	1,923,202	1,283,202	640,000	23,059,204	5,120,000	3,196,800

Note that two scenarios are considered that are characterized by one (Test 1a) and four order of magnitude (Test 1b) contrast in Young's modulus between material 1 (stiff) and 2 (soft), respectively. We define the following characteristic consolidation time $t_c^{(T_1)}$ associated with the consolidation process [84]:

$$t_c^{(T_1)} = \frac{L^2}{\lambda(\kappa_1)} \frac{(1+\nu)(1-2\nu)}{E(1-\nu)}, \quad (30)$$

where the mobility is evaluated using the permeability of material 1.

The domain is discretized using three different mesh types, which are labeled as: `cart`, `rand_1`, and `rand_2`. The base mesh for each family are shown in Fig. 2 and consist of 100×100 quadrilateral elements. Three refined meshes generated by dyadic subdivision are considered for each family, with $\ell \in \{0, 1, 2, 3\}$ indicating the refinement level. The notation (ℓ) is used to denote the refinement level of a given mesh. As an example, `cart(2)` is the mesh belonging to family `cart` obtained after two levels of refinement. Table 2 provides dimensions and non-zeros of the fine scale system matrix blocks for each refinement level. Note that for a given refinement level sparsity patterns are the same for any mesh family. The coarse problem is always constructed based on a coarsening ratio (C.R.)—namely, the ratio between number of fine grid elements and coarse grid elements—equal to 100. Practically, the coarse-grid is constructed agglomerating evenly 10 fine-scale elements in both ξ_1 - and ξ_2 -direction. Table 3 reports the dimensions of the coarse system \mathbf{A}_n^H . IC(0) factorizations are used for both \tilde{A} and \tilde{S} . We consider two different timestep values, i.e. $\Delta t_1/t_c^{(T_1)} = 1 \times 10^{-1}$ and $\Delta t_2/t_c^{(T_1)} = 1 \times 10^{-2}$.

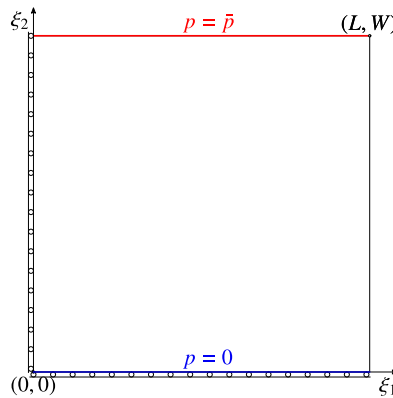


Fig. 1: Test 1: Physical domain.

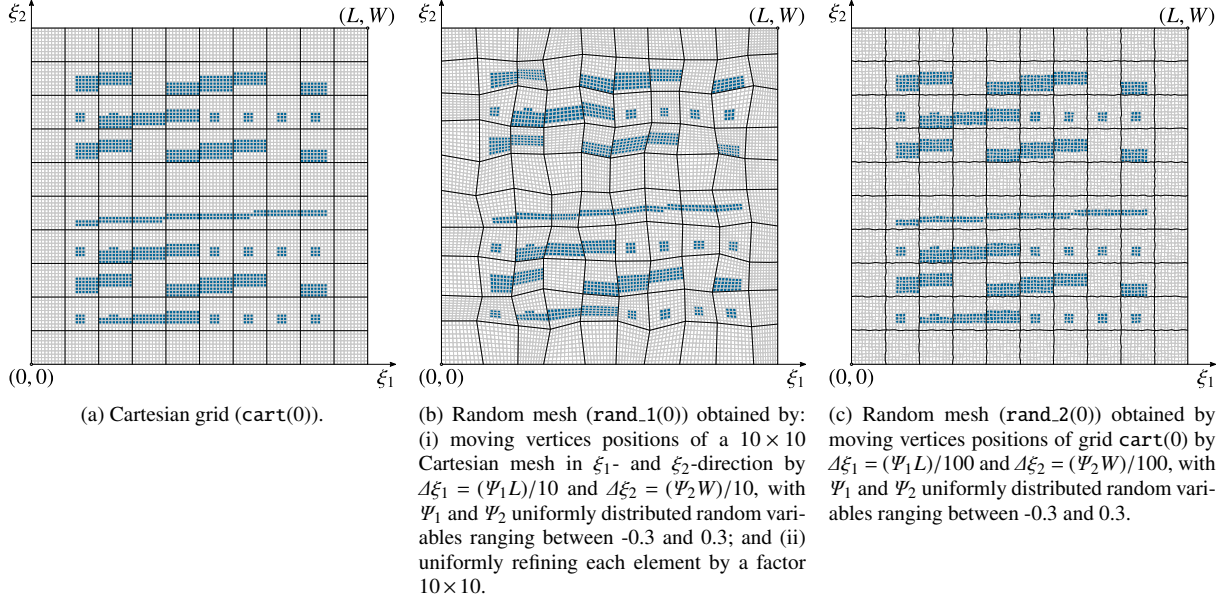


Fig. 2: Test 1: Physical domain (a) and different base meshes in thin gray lines (b,c,d) used in the numerical tests. Each mesh consists 100×100 quadrilateral elements ($\ell = 0$ in Table 2). The bold black lines identify fine-scale element aggregates that define coarse-scale elements using a coarsening ratio $\text{C.R.} = 10 \times 10$. The blue color in (b,c,d) denotes fine-scale cell belonging to the material 2 region [12].

Table 3: Test 1: Size of the coarse grid problem assuming a coarsening ratio $\text{C.R.} = 10 \times 10$ as a function of mesh refinement level (ℓ). The total number of fine scale DOFs is $n_t^H = n_u^H + n_p^H$.

ℓ	n_e^H	n_t^H	n_u^H	n_p^H
0	10×10	342	242	100
1	20×20	1,282	882	400
2	40×40	4,962	3,362	1,600
3	80×80	19,522	13,122	6,400

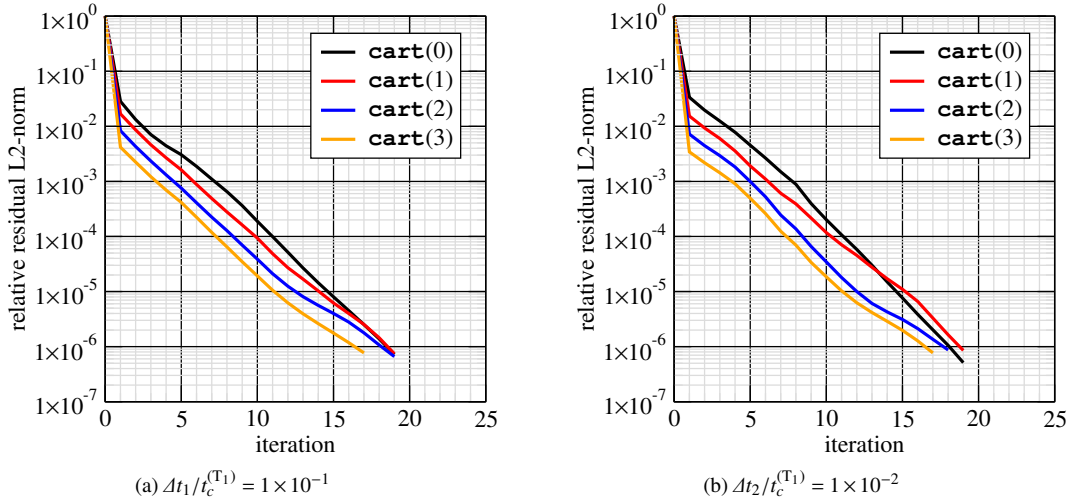


Fig. 3: Test 1a: \mathbf{M}_n^{-1} -preconditioned GMRES convergence profile as a function of the refinement level ℓ for mesh family $\text{cart}(\ell)$, $\ell = \{0, 1, 2, 3\}$, using two different timestep sizes. The no-fill $\text{IC}(0)$ preconditioner is used for both $\tilde{\mathbf{A}}^{-1}$ and $\tilde{\mathbf{S}}^{-1}$.

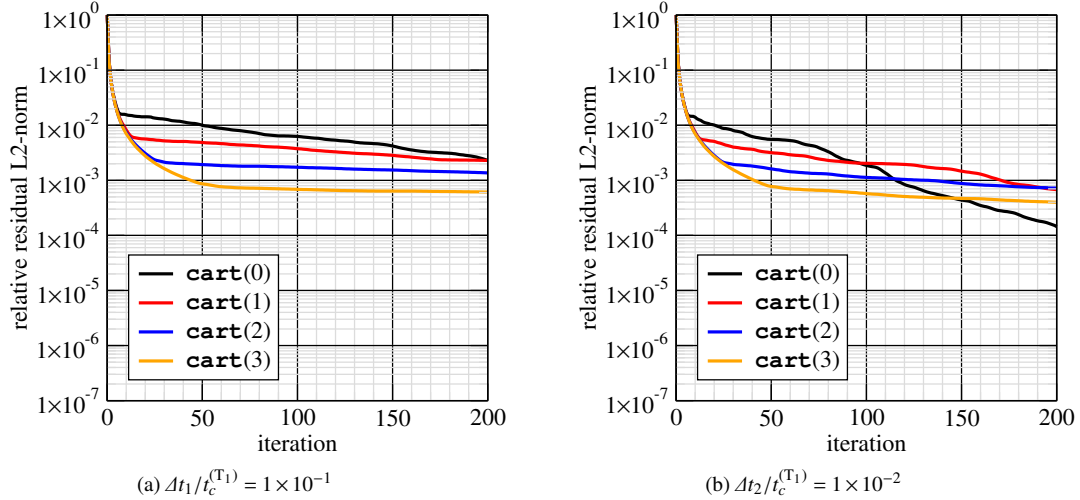
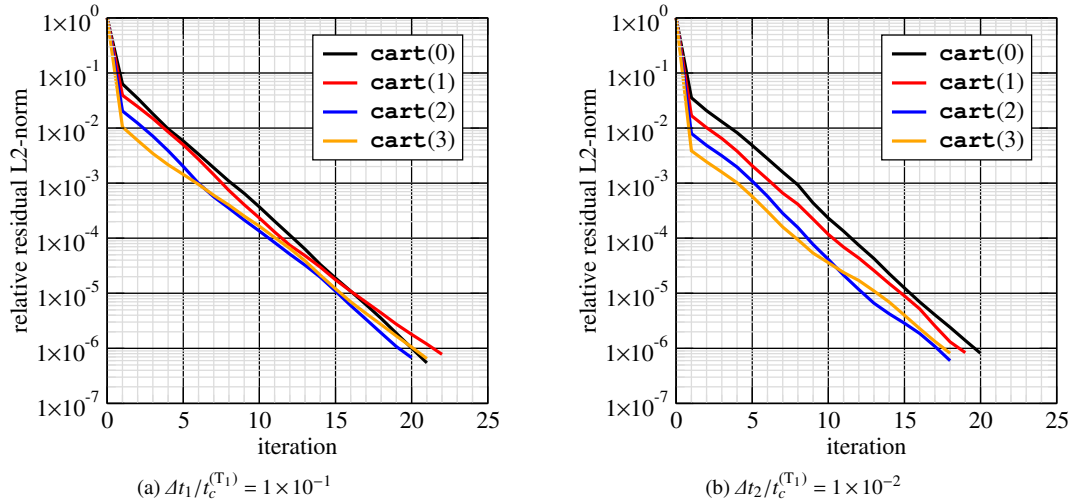
Fig. 4: Test 1a: Same as Fig. 3 for \mathbf{M}_L^{-1} -preconditioned GMRES.

Fig. 5: Test 1b: Same as Fig. 3.

The benefits from the proposed multiscale-based two-stage preconditioner are first demonstrated by comparing the performance of \mathbf{M}_n^{-1} -preconditioned GMRES with that of GMRES preconditioned by the local preconditioner \mathbf{M}_L^{-1} only for the first timestep of the simulation. Full GMRES (no restart) is used with maximum number of iterations $n_{\text{iter}}^{\text{max}} = 200$. We focus on mesh family `cart`. Figs. 3-4 display the convergence profile for the relative residual norm in Test 1a. The two-stage preconditioning approach (Fig. 3) allows for convergence in a number of iteration varying between 17 and 19 and exhibits practically no dependence on the mesh and timestep size. For the most refined mesh `cart(3)`, the overall time (preconditioner setup + solution time) to compute the solution is about 20 seconds for both timestep sizes, the global and local preconditioner densities being $\rho_G = 0.782$ and $\rho_L = 0.896$. Conversely, the only use of the local preconditioner (Fig. 4) does not reduce the residual to the requested tolerance, with a convergence profile that tends to stagnate for both meshes `cart(2)` and `cart(3)`. A similar behavior is observed for Test 1b (See Figs. 5a-5b). As observed in Remark 2, an alternative approach consists of using better quality local preconditioners for the elasticity stiffness matrix and the Schur complement to improve the convergence behavior of \mathbf{M}_L -preconditioned GMRES. As theoretical reference we provide the best performance in terms of iteration count that is obtained when A^{-1} and S_{FS}^{-1} in (20) are applied exactly using inner solvers: (i) in Test 1a, convergence is always obtained within 5 to 7 iterations; (ii) in Test 1b, up to about 70 iterations may be required to achieve the requested tolerance, the iteration counts being higher for the smaller timestep size. This confirms that a multiscale two-stage approach is particularly effective in complementing the action of the diagonal fixed-stress Schur complement approximation for media characterized by high stiffness contrasts.

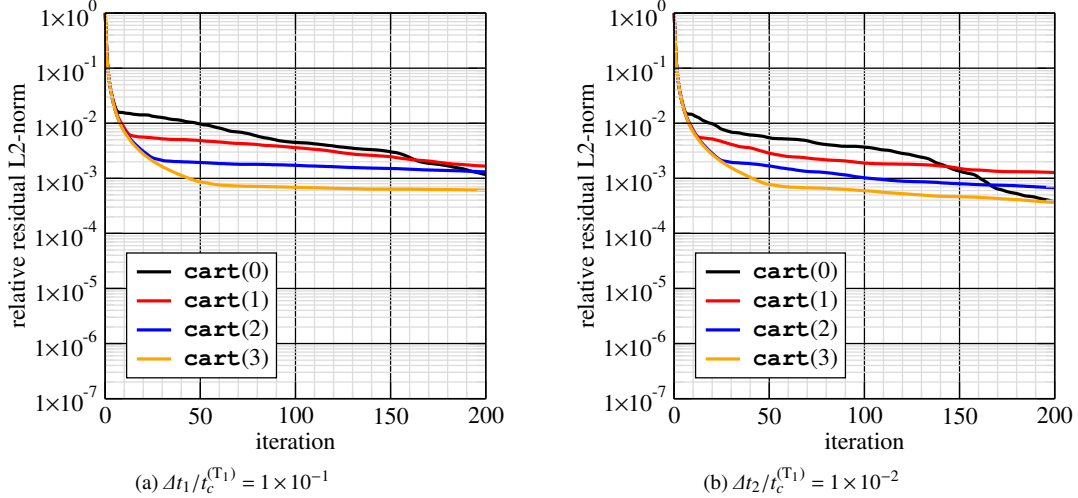


Fig. 6: Test 1b: Same as Fig. 4.

Table 4: Test 1a: preconditioner densities, average number of iterations and timings as a function of the refinement level for the three mesh families using two different timestep sizes. The total number of timesteps is 10 in all cases. The coarse grid problem is constructed assuming a coarsening ratio C.R. = 10×10 . No-fill IC(0) preconditioners are used for \tilde{A}^{-1} and \tilde{S}^{-1} .

mesh	ρ_G	ρ_L	ρ_r	$\Delta t_1/t_c^{(T_1)} = 1 \times 10^{-1}$				$\Delta t_2/t_c^{(T_1)} = 1 \times 10^{-2}$			
				n_{iter}	T_p [s]	\bar{T}_s [s]	\bar{T}_t [s]	n_{iter}	T_p [s]	\bar{T}_s [s]	\bar{T}_t [s]
cart(0)	0.668	0.897	2.565	19.0	0.3	0.1	0.4	18.1	0.3	0.1	0.4
cart(1)	0.702	0.896	2.598	19.0	0.7	0.5	1.1	18.5	0.7	0.4	1.1
cart(2)	0.738	0.896	2.634	19.0	2.7	2.1	4.8	18.5	2.7	2.0	4.7
cart(3)	0.782	0.896	2.678	17.7	11.8	8.4	20.1	17.0	11.8	8.2	20.0
rand.1(0)	0.672	0.913	2.585	17.1	0.3	0.1	0.4	17.1	0.3	0.1	0.4
rand.1(1)	0.704	0.913	2.617	18.2	0.7	0.4	1.1	19.0	0.7	0.5	1.1
rand.1(2)	0.740	0.913	2.652	18.7	2.8	2.1	4.9	18.0	2.8	2.0	4.8
rand.1(3)	0.775	0.912	2.688	17.3	12.1	8.5	20.5	17.0	12.0	8.3	20.3
rand.2(0)	0.672	0.913	2.585	18.0	0.3	0.1	0.4	17.2	0.3	0.1	0.4
rand.2(1)	0.705	0.913	2.617	18.0	0.7	0.4	1.1	17.7	0.7	0.4	1.1
rand.2(2)	0.740	0.913	2.652	18.0	2.8	2.0	4.8	17.5	2.8	1.9	4.7
rand.2(3)	0.775	0.912	2.688	16.7	12.1	7.8	19.9	16.0	12.1	7.8	19.9

Table 5: Test 1b:same as Table 4.

mesh	ρ_G	ρ_L	ρ_r	$\Delta t_1/t_c^{(T_1)} = 1 \times 10^{-1}$				$\Delta t_2/t_c^{(T_1)} = 1 \times 10^{-2}$			
				n_{iter}	T_p [s]	\bar{T}_s [s]	\bar{T}_t [s]	n_{iter}	T_p [s]	\bar{T}_s [s]	\bar{T}_t [s]
cart(0)	0.668	0.897	2.565	21.7	0.3	0.2	0.5	19.5	0.3	0.1	0.4
cart(1)	0.702	0.896	2.598	24.1	0.7	0.6	1.3	20.6	0.7	0.5	1.2
cart(2)	0.738	0.896	2.634	22.1	2.8	2.4	5.2	18.5	2.8	2.0	4.8
cart(3)	0.782	0.896	2.678	23.1	11.7	11.4	23.1	19.7	11.7	9.6	21.3
rand.1(0)	0.672	0.913	2.585	21.3	0.3	0.1	0.5	19.0	0.3	0.1	0.5
rand.1(1)	0.704	0.913	2.617	23.3	0.7	0.4	1.3	19.7	0.7	0.5	1.2
rand.1(2)	0.740	0.913	2.652	22.2	2.9	2.4	5.3	18.1	2.9	2.0	4.9
rand.1(3)	0.775	0.912	2.688	25.0	12.1	12.7	24.8	21.1	12.1	9.3	21.4
rand.2(0)	0.672	0.913	2.585	20.6	0.3	0.1	0.4	18.5	0.3	0.1	0.4
rand.2(1)	0.705	0.913	2.617	23.1	0.7	0.6	1.3	19.7	0.7	0.5	1.2
rand.2(2)	0.740	0.913	2.652	21.0	2.9	2.4	5.3	17.6	2.9	2.0	4.9
rand.2(3)	0.775	0.912	2.688	21.9	12.1	11.1	23.2	18.6	12.1	7.8	20.0

Table 6: Test 2: simulation parameters. Fluid viscosity has a constant value $\mu = 1 \times 10^{-3}$ Pa·s.

Symbol	Quantity	Underburden	Reservoir	Overburden	Unit
E	Young's modulus	5×10^{10}	(see Eq. (31))	5×10^{10}	[Pa]
ν	Poisson's ratio	0.25	0.25	0.25	[-]
κ	isotropic permeability	—	(see Fig. 7b)	—	[m ²]
L	region size in ξ_1 -direction	762.0	762.0	762.0	[m]
W_i	region size in ξ_2 -direction, $i \in \{U, R, O\}$	30.48	15.24	30.48	[m]
H	region size in ξ_3 -direction	30.48	15.24	30.48	[m]
\bar{p}	prescribed pressure (see Figs. 7a)	—	1×10^6	—	[Pa]

Table 7: Test 2: Size and numbers of non-zero elements in the system matrix blocks as a function of mesh refinement level (ℓ). The number of fine scale elements n_e refers to the mechanical problem. Flow is allowed for only in the reservoir region (see Fig. 7) that includes one fifth of the cells in the ξ_2 -direction. The total number of fine scale DOFs is $n_t = n_u + n_p$.

ℓ	n_e	n_t	n_u	n_p	nnz(A)	nnz(B)	nnz(C)
0	100×100	22,402	20,402	2,000	362,404	16,000	9,760
1	200×200	88,802	80,802	8,000	1,444,804	64,000	39,520
2	400×400	353,602	321,602	32,000	5,769,604	256,000	159,040
3	800×800	1,411,202	1,283,202	128,000	23,059,204	1,024,000	638,080

The behavior observed for mesh family *cart* is representative of the performance of the two-stage preconditioner also for the other mesh families. Tables 4–5 report preconditioner densities, number of iterations and timings averaged over 10 timesteps as a function of the refinement level ℓ . GMRES always exhibits robust convergence.

Test 2: Heterogeneous synthetic reservoir

Here, flow in a highly heterogeneous deforming reservoirs is modeled. We focus on a two-dimensional domain, for which plane-strain conditions are assumed. The setup is based on model one in the 10th SPE Comparative Solution Project [22] but equipped with poroelastic mechanical behavior. Incompressible fluid and solid constituents are assumed. In particular, Young's modulus is correlated to the permeability according to the following relationship:

$$E = E_{\max} + \gamma \cdot \{\log_{10}(\kappa) - \min[\log_{10}(\kappa)]\}, \quad (31)$$

with

$$\gamma = \frac{\bar{E} - E_{\max}}{\text{mean}[\log_{10}(\kappa)] - \min[\log_{10}(\kappa)]} \quad (32)$$

where mean is the operator returning the average value, $\bar{E} = 5 \times 10^9$ Pa, and $E_{\max} = 1.5\bar{E}$ the largest Young's modulus value, which is assigned to elements having the lowest permeability. The Poisson ratio is set to 0.25 everywhere. Based on Eq.(30), we define a characteristic consolidation time $t_c^{(\Gamma_2)}$ that is computed using \bar{E} and an appropriate permeability value $\bar{\kappa}$, i.e. setting $\lambda = \bar{\kappa}/\mu$. Here, the permeability is cell-wise isotropic and we set $\bar{\kappa} = \max(\kappa)$, which leads to $t_c^{(\Gamma_2)} = 1.14$ days. The simulation parameters are summarized in Table 6.

The computational domain consists of two nested regions as shown in Figs.7c-7d. The pressure field is computed only in the reservoir region, i.e., domain Ω^F , assuming impermeable over-burden and under-burden units. The displacement field is simulated over the domain Ω^M that includes reservoir, overburden and underburden. Practically, on $\Omega^M \setminus \Omega^F$ drained conditions are assumed, i.e. the pressure term in Eq.(1a) vanishes. The reservoir region is 762 m long and 15.24 m thick. Overburden and underburden are twice as thick as the reservoir. Roller support and zero flux conditions are prescribed at the entire boundary except for the two segments highlighted in red and blue in Figure 6a where Dirichlet pressure conditions

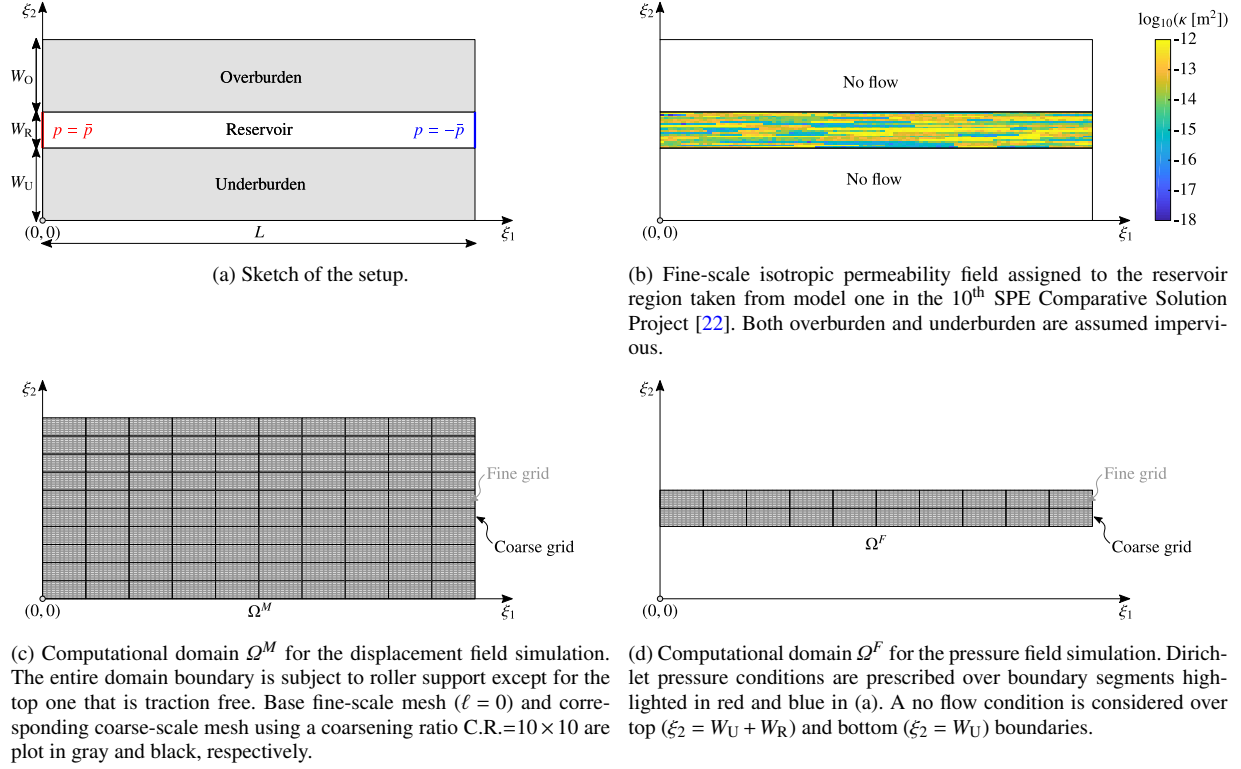


Fig. 7: Test 2: Two-dimensional heterogeneous synthetic reservoir.

Table 8: Test 2: Size of the coarse grid problem assuming a coarsening ratio C.R.= 10×10 as a function of mesh refinement level (ℓ). The total number of fine scale DOFs is $n_t^H = n_u^H + n_p^H$.

ℓ	n_e^H	n_t^H	n_u^H	n_p^H
0	10×10	262	242	20
1	20×20	962	882	80
2	40×40	3,682	3,362	320
3	80×80	14,402	13,122	1,280

Table 9: Test 2: Preconditioner densities, average number of iterations and timings as a function of the refinement level (ℓ) using two different timestep sizes. The total number of timesteps is 10 in all cases. The coarse grid problem is constructed assuming a coarsening ratio C.R. = 10×10 . The local preconditioners are $\tilde{A}^{-1} = A_{\text{IC}(0)}^{-1}$ and $\tilde{S}^{-1} = S_{\text{FS,IC}(0)}^{-1}$.

ℓ	ρ_G	ρ_L	ρ_t	$\Delta t_1/t_c^{(\text{T}2a)} = 1 \times 10^{-1}$				$\Delta t_2/t_c^{(\text{T}2a)} = 1 \times 10^{-3}$			
				n_{iter}	T_p [s]	\bar{T}_s [s]	\bar{T}_t [s]	n_{iter}	T_p [s]	\bar{T}_s [s]	\bar{T}_t [s]
0	0.834	1.039	2.873	28.3	0.3	0.1	0.5	18.9	0.3	0.1	0.5
1	0.857	1.040	2.897	35.4	0.6	0.6	1.2	25.3	0.6	0.4	1.0
2	0.885	1.040	2.925	29.3	2.5	2.2	4.7	31.3	2.5	2.4	5.0
3	0.921	1.040	2.961	28.5	10.5	9.8	20.3	35.2	10.5	12.8	23.3

apply. The simulation parameters are indicated in Table 6. Proceeding as in Test 1, we consider a base regular grid consisting of 100×100 regular quadrilateral elements with an aspect ratio of 10, i.e. the same grid element defined in [22]. Then, three refinement levels are considered. Again, the coarse mesh is always obtained using a coarsening ratio of 10×10 . Size and number of non-zeroes elements characterizing the fine-scale and the coarse-scale matrices are given in Tables 7-8.

Table 9 presents the behavior of the preconditioner as a function of the grid-refinement level ℓ and timestep size. The average number of iterations and timings are obtained using 10 timesteps. Despite the milder stiffness contrast compared to Test 1, the combination of unfavorable aspect ratio of the elements and highly heterogeneous distributions of the permeability

Table 10: Test 2: Preconditioner densities, average number of iterations and timings as a function of the refinement level (ℓ) for GMRES preconditioned using different strategies. The smaller timestep size Δt_2 of Table 9 is selected. The total number of timesteps is 10 in all cases. The coarse grid problem is constructed assuming a coarsening ratio C.R. = 10×10 . The local preconditioners are $\tilde{A}^{-1} = A_{\text{IC}(0)}^{-1}$ and $\tilde{S}^{-1} = S_{\text{FS,ICT}(\tau_S)}^{-1}$, with $\tau_S = 1 \times 10^{-3}$.

ℓ	Block-triangular preconditioner with inner solvers for A^{-1} and S_{FS}^{-1}			Two-stage multiscale preconditioner					Block-triangular preconditioner with incomplete factorizations for A^{-1} and S_{FS}^{-1}			
	ρ_G	ρ_L	n_{iter}	ρ_t	n_{iter}	T_p [s]	\bar{T}_s [s]	\bar{T}_t [s]	n_{iter}	T_p [s]	\bar{T}_s [s]	\bar{T}_t [s]
0	0.834	1.054	8.0	2.887	16.0	0.2	0.1	0.3	46.3	0.0	0.2	0.2
1	0.857	1.056	7.9	2.913	14.2	0.6	0.2	0.8	73.6	0.0	1.0	1.0
2	0.885	1.060	6.7	2.945	13.1	2.5	1.0	3.5	97.3	0.1	6.6	6.6
3	0.921	1.057	5.0	2.978	15.2	10.4	4.9	15.3	172.8	0.2	75.1	75.3

field makes the solution of this problem much more challenging than the one addressed in Test 1. Even though the solver does exhibit mild dependence on ℓ , in particular for the smaller timestep value, the average number of iterations remains well bounded. Given the severe jumps in permeability, improving the Schur complement local preconditioner using an ICT-based factorization proves beneficial. In Table 10 the performance of GMRES preconditioned by the multiscale two-stage preconditioner is compared with that of GMRES combined with the local preconditioner only. Again, the iteration count obtained applying \tilde{A}^{-1} and $\tilde{S}_{\text{FS}}^{-1}$ exactly in a block triangular preconditioner is provided as theoretical reference. Note the reduction by 50% of the number of iterations required at every mesh level by GMRES preconditioned by the multiscale two-stage strategy, hence the practical advantage of a much lower-dimensional basis for the Krylov space that has to be stored as the iteration progresses. Despite the higher cost per iteration, the gain in iteration count is such that the average solution time \bar{T}_s is also essentially halved. Although the local preconditioner \mathbf{M}_L^{-1} allows for achieving the desired convergence, it is not competitive with the two-stage approach and exhibits mesh dependent behavior.

5 Conclusions

We described a two-stage preconditioner for the displacement-pressure formulation of the Biot poroelasticity equations. The preconditioner is used to accelerate a non-symmetric Krylov solver. The preconditioner features are: (i) the construction of accurate coarse-scale coupled systems based on multiscale formulations; and (ii) a local smoothing preconditioner that takes the form a block triangular operator. Based on a two-grid approach—where a much coarser grid is superimposed on the original fine-scale one—, distinct sets of multiscale basis functions are computed for the displacement and pressure fields solving local Dirichlet problems. By assembling such basis functions in a global block diagonal multiscale prolongation operator, a Galerkin projection is used to construct upscaled (coarse-scale) coupled systems that are much simpler to solve for. When applied as a right preconditioner for GMRES, the proposed two-stage solver shows robust performance for problems involving highly heterogeneous material property fields. Mild mesh-dependent convergence is observed in a sequence of refined problems for the heterogeneous case. Overall, the analysis builds confidence in the proposed multiscale-based two-stage preconditioning strategy as a sound basis for the design of reliable and efficient solvers. Current work is focused on the extensions to three-dimensional problems and general unstructured grids.

Acknowledgements N. Castelletto, S. Klevtsov and H.A. Tchelepi gratefully acknowledge the financial support provided by the Reservoir Simulation Industrial Affiliates Consortium at Stanford University (SUPRI-B) and Total S.A. through the Stanford Total Enhanced Modeling of Source rock (STEMS) project. H. Hajibeygi was sponsored by Schlumberger Petroleum Services CV, The Netherlands. The authors also thank Andrea Franceschini for his insightful suggestions. Portions of this work were performed under the auspices of the U.S. Department of Energy by Lawrence Livermore National Laboratory under Contract DE-AC52-07 NA27344.

References

1. Adler J. H. Gaspar, F.J., Hu, X., Rodrigo, C., Zikatanov, L.T.: Robust Block Preconditioners for Biot’s Model. In: P.E. Bjøstad, S. Brenner, L. Halpern, R. Kornhuber, H.H. Kim, T. Rahman, O.B. Widlund (eds.) Domain Decomposition Methods in Science and Engineering XXIV, pp. xxx–xxx. Springer International Publishing (2018). DOI 10.1007/978-3-319-93873-8
2. Akkutlu, I.Y., Efendiev, Y., Vasilyeva, M., Wang, Y.: Multiscale model reduction for shale gas transport in poroelastic fractured media. *J. Comput. Phys.* **353**, 356–376 (2018). DOI 10.1016/j.jcp.2017.10.023
3. Aziz, K., Settari, A.: *Petroleum Reservoir Simulation*. Elsevier Applied Science Publishers, London, UK (1979)

4. Bause, M., Radu, F.A., Köcher, U.: Spacetime finite element approximation of the Biot poroelasticity system with iterative coupling. *Comput. Meth. Appl. Mech. Eng.* **320**, 745–768 (2017). DOI 10.1016/j.cma.2017.03.017
5. Benzi, M.: Preconditioning Techniques for Large Linear Systems: A Survey. *J. Comput. Phys.* **182**(2), 418–477 (2002). DOI 10.1006/jcph.2002.7176
6. Benzi, M., Golub, G.H., Liesen, J.: Numerical solution of saddle point problems. *Acta Numer.* **14**, 1–137 (2005). DOI 10.1017/S0962492904000212
7. Bergamaschi, L., Ferronato, M., Gambolati, G.: Novel preconditioners for the iterative solution to FE-discretized coupled consolidation equations. *Comp. Meth. Appl. Mech. Eng.* **196**(25–28), 2647–2656 (2007). DOI 10.1016/j.cma.2007.01.013
8. Bergamaschi, L., Martínez, Á.: RMCP: Relaxed Mixed Constraint Preconditioners for saddle point linear systems arising in geomechanics. *Comp. Meth. Appl. Mech. Eng.* **221–222**, 54–62 (2012). DOI 10.1016/j.cma.2012.02.004
9. Both, J.W., Borregales, M., Nordbotten, J.M., Kumar, K., Radu, F.A.: Robust fixed stress splitting for Biot’s equations in heterogeneous media. *Appl. Math. Lett.* **68**, 101–108 (2017). DOI 10.1016/j.aml.2016.12.019
10. Both, J.W., Kumar, K., Nordbotten, J.M., Radu, F.A.: Anderson accelerated fixed-stress splitting schemes for consolidation of unsaturated porous media (2018)
11. Bramble, J.H., Pasciak, J.E.: A preconditioning technique for indefinite systems resulting from mixed approximations of elliptic problems. *Math. Comput.* **50**(181), 1–17 (1988). DOI 10.1090/S0025-5718-1988-0917816-8
12. Brown, D.L., Vasilyeva, M.: A Generalized Multiscale Finite Element Method for poroelasticity problems I: Linear problems. *J. Comput. Appl. Math.* **294**, 372–388 (2016). DOI 10.1016/j.cam.2015.08.007
13. Brown, D.L., Vasilyeva, M.: A Generalized Multiscale Finite Element Method for poroelasticity problems II: Nonlinear coupling. *J. Comput. Appl. Math.* **297**, 132–146 (2016). DOI 10.1016/j.cam.2015.11.007
14. Buck, M., Iliev, O., Andrä, H.: Multiscale finite element coarse spaces for the application to linear elasticity. *Cent. Eur. J. Math.* **11**(4), 680–701 (2013). DOI 10.2478/s11533-012-0166-8
15. Buck, M., Iliev, O., Andrä, H.: Multiscale Finite Elements for Linear Elasticity: Oscillatory Boundary Conditions. In: J. Erhel, J.M. Gander, L. Halpern, G. Pichot, T. Sassi, O. Widlund (eds.) *Domain Decomposition Methods in Science and Engineering XXI*, pp. 237–245. Springer International Publishing (2014). DOI 10.1007/978-3-319-05789-7_20
16. Cao, H., Tchelepi, H.A., Wallis, J., Yardumian, H.: Parallel scalable unstructured CPR-type linear solver for reservoir simulation. In: *Proceedings - SPE Annual Technical Conference and Exhibition. Society of Petroleum Engineers* (2005). DOI 10.2118/173226-MS
17. Castelletto, N., Ferronato, M., Gambolati, G.: Thermo-hydro-mechanical modeling of fluid geological storage by Godunov-mixed methods. *Int. J. Numer. Meth. Eng.* **90**(8), 988–1009 (2012). DOI 10.1002/nme.3352
18. Castelletto, N., Hajibeygi, H., Tchelepi, H.: Hybrid Multiscale Formulation for Coupled Flow and Geomechanics. In: *Proceedings of the 15th European Conference on the Mathematics of Oil Recovery (ECMOR XV)*. EAGE (2016). DOI 10.3997/2214-4609.201601888
19. Castelletto, N., Hajibeygi, H., Tchelepi, H.: Multiscale Finite-Element Method for Linear Elastic Geomechanics. *J. Comput. Phys.* **331**, 337–356 (2017). DOI 10.1016/j.jcp.2016.11.044
20. Castelletto, N., White, J.A., Ferronato, M.: Scalable algorithms for three-field mixed finite element coupled poromechanics. *J. Comput. Phys.* **327**, 894–918 (2016). DOI 10.1016/j.jcp.2016.09.063
21. Castelletto, N., White, J.A., Tchelepi, H.A.: Accuracy and convergence properties of the fixed-stress iterative solution of two-way coupled poromechanics. *Int. J. Numer. Anal. Methods Geomech.* **39**(14), 1593–1618 (2015). DOI 10.1002/nag.2400
22. Christie, M., Blunt, M.: Tenth SPE comparative solution project: A comparison of upscaling techniques. *SPE Reserv. Eval. Eng.* **4**(4), 308–316 (2001). DOI 10.2118/72469-PA
23. Coussy, O.: *Poromechanics*. Wiley, Chichester, UK (2004)
24. Cusini, M., Fryer, B., van Kruijsdijk, C., Hajibeygi, H.: Algebraic dynamic multilevel method for compositional flow in heterogeneous porous media. *J. Comput. Phys.* **354**, 593–612 (2018). DOI 10.1016/j.jcp.2017.10.052
25. Cusini, M., Lukyanov, A.A., Natvig, J., Hajibeygi, H.: Constrained pressure residual multiscale (CPR-MS) method for fully implicit simulation of multiphase flow in porous media. *J. Comput. Phys.* **299**, 472–486 (2015). DOI 10.1016/j.jcp.2015.07.019
26. Dana, S., Ganis, B., Wheeler, M.F.: A multiscale fixed stress split iterative scheme for coupled flow and poromechanics in deep subsurface reservoirs. *J. Comput. Phys.* **352**, 1–22 (2018). DOI 10.1016/j.jcp.2017.09.049
27. Di Pietro, D.A., Eymard, R., Lemaire, S., Masson, R.: Hybrid Finite Volume Discretization of Linear Elasticity Models on General Meshes. In: J. Foft et al. (ed.) *Finite Volumes for Complex Applications VI Problems & Perspectives*, pp. 331–339. Springer-Verlag, Berlin (2011)
28. Droniou, J.: Finite volume schemes for diffusion equations: introduction to and review of modern methods. *Math. Models Meth. Appl. Sci.* **24**(8), 1575–1619 (2014). DOI 10.1142/S0218202514400041
29. Efendiev, Y., Hou, T.Y.: *Multiscale Finite Element Methods: Theory and Applications*. Springer, New York, NY, USA (2009). DOI 10.1007/978-0-387-09496-0
30. Eymard, R., Gallouët, T., Guichard, C., Herbin, R., Masson, R.: TP or not TP, that is the question. *Comput. Geosci.* **18**(3), 285–296 (2014). DOI 10.1007/s10596-013-9392-9
31. Eymard, R., Gallouët, T., Herbin, R.: Finite Volume Methods. In: P.G. Ciarlet, J.L. Lions (eds.) *Handbook of Numerical Analysis*, vol. 7, pp. 713–1018. Elsevier (2000). DOI 10.1016/S1570-8659(00)07005-8
32. Ferronato, M., Castelletto, N., Gambolati, G.: A fully coupled 3-D mixed finite element model of Biot consolidation. *J. Comput. Phys.* **229**(12), 4813–4830 (2010). DOI 10.1016/j.jcp.2010.03.018
33. Frijns, A.J.H.: A four-component mixture theory applied to cartilaginous tissues: numerical modelling and experiments. Phd thesis, Technische Universiteit Eindhoven, The Netherlands (2000)
34. Gai, X., Sun, S., Wheeler, M.F., Klie, H.: A Time-Stepping Scheme for Coupled Reservoir Flow and Geomechanics. In: *Proceedings - SPE Annual Technical Conference and Exhibition. Society of Petroleum Engineers* (2005). DOI 10.2118/97054-MS
35. Gaspar, F.J., Lisbona, F.J., Oosterlee, C.W., Wienands, R.: A systematic comparison of coupled and distributive smoothing in multigrid for the poroelasticity system. *Numer. Linear Algebr. Appl.* **11**(2-3), 93–113 (2004). DOI 10.1002/nla.372
36. Gaspar, F.J., Rodrigo, C.: On the fixed-stress split scheme as smoother in multigrid methods for coupling flow and geomechanics. *Comput. Meth. Appl. Mech. Eng.* **326**, 526–540 (2017). DOI 10.1016/j.cma.2017.08.025
37. Haga, J.B., Osnes, H., Langtangen, H.P.: A parallel block preconditioner for large-scale poroelasticity with highly heterogeneous material parameters. *Comput. Geosci.* **16**(3), 723–734 (2012). DOI 10.1007/s10596-012-9284-4
38. Haga, J.B., Osnes, H., Langtangen, H.P.: On the causes of pressure oscillations in low-permeable and low-compressible porous media. *Int. J. Numer. Anal. Methods Geomech.* **36**(12), 1507–1522 (2012). DOI 10.1002/nag.1062

39. Hajibeygi, H., Bonfigli, G., Hesse, M.A., Jenny, P.: Iterative multiscale finite-volume method. *J. Comput. Phys.* **227**(19), 8604–8621 (2008). DOI 10.1016/j.jcp.2008.06.013
40. Helmig, R., Niessner, J., Flemisch, B., Wolff, M., Fritz, J.: Efficient Modeling of Flow and Transport in Porous Media Using Multiphysics and Multiscale Approaches. In: W. Freeden, M.Z. Nashed, T. Sonar (eds.) *Handbook of Geomathematics*, pp. 417–457. Springer Berlin Heidelberg, Berlin, Heidelberg (2010). DOI 10.1007/978-3-642-01546-5_15
41. Hou, T.Y., Wu, X.H.: A Multiscale Finite Element Method for Elliptic Problems in Composite Materials and Porous Media. *J. Comput. Phys.* **134**(1), 169–189 (1997). DOI 10.1006/jcph.1997.5682
42. Hu, X., Rodrigo, C., Gaspar, F.J., Zikatanov, L.T.: A nonconforming finite element method for the Biot's consolidation model in poroelasticity. *J. Comput. Appl. Math.* **310**, 143–154 (2017). DOI 10.1016/j.cam.2016.06.003
43. Hughes, T.J.R.: *The Finite Element Method: Linear Static and Dynamic Finite Element Analysis*. Dover Publications (2000)
44. Jenny, P., Lee, S.H., Tchelepi, H.A.: Multi-scale finite-volume method for elliptic problems in subsurface flow simulation. *J. Comput. Phys.* **187**(1), 47–67 (2003). DOI 10.1016/S0021-9991(03)00075-5
45. Jenny, P., Lee, S.H., Tchelepi, H.A.: Adaptive fully implicit multi-scale finite-volume method for multi-phase flow and transport in heterogeneous porous media. *J. Comput. Phys.* **217**(2), 627–641 (2006). DOI 10.1016/j.jcp.2006.01.028
46. Jha, B., Juanes, R.: A locally conservative finite element framework for the simulation of coupled flow and reservoir geomechanics. *Acta Geotech.* **2**(3), 139–153 (2007). DOI 10.1007/s11440-007-0033-0
47. Jha, B., Juanes, R.: Coupled multiphase flow and poromechanics: A computational model of pore pressure effects on fault slip and earthquake triggering. *Water Resour. Res.* **5**, 3776–3808 (2014). DOI 10.1002/2013WR015175
48. Kalchev, D.Z., Lee, C.S., Villa, U., Efendiev, Y., Vassilevski, P.S.: Upscaling of Mixed Finite Element Discretization Problems by the Spectral AMG Method. *SIAM J. Sci. Comput.* **38**(5), A2912–A2933 (2016). DOI 10.1137/15M1036683
49. Keilegavlen, E., Nordbotten, J.M.: Finite volume methods for elasticity with weak symmetry. *Int. J. Numer. Meth. Eng.* **112**, 939–962 (2017). DOI 10.1002/nme.5538
50. Kim, J., Tchelepi, H.A., Juanes, R.: Stability, accuracy and efficiency of sequential methods for coupled flow and geomechanics. *SPE J.* **16**(2), 249–262 (2011). DOI 10.2118/119084-PA
51. Kim, J., Tchelepi, H.A., Juanes, R.: Stability and convergence of sequential methods for coupled flow and geomechanics: Fixed-stress and fixed-strain splits. *Comput. Meth. Appl. Mech. Eng.* **200**(13), 1591–1606 (2011). DOI 10.1016/j.cma.2010.12.022
52. Klevtsov, S., Castelletto, N., White, J., Tchelepi, H.: Block-preconditioned Krylov Methods for Coupled Multiphase Reservoir Flow and Geomechanics. In: *Proceedings of the 15th European Conference on the Mathematics of Oil Recovery (ECMOR XV)*. EAGE (2016). DOI 10.3997/2214-4609.201601900
53. Kozlova, A., Li, Z., Natvig, J.R., Watanabe, S., Zhou, Y., Bratvedt, K., Lee, S.H.: A Real-Field Multiscale Black-Oil Reservoir Simulator. In: *SPE Reservoir Simulation Symposium*. Society of Petroleum Engineers (2015). DOI 10.2118/173226-MS
54. Lee, J.J., Mardal, K.A., Winther, R.: Parameter-Robust Discretization and Preconditioning of Biot's Consolidation Model. *SIAM J. Sci. Comput.* **39**(1), A1–A24 (2010). DOI 10.1137/15M1029473
55. Lewis, R.W., Schrefler, B.A.: *The Finite Element Method in the Static and Dynamic Deformation and Consolidation of Porous Media*, 2nd edn. Wiley, Chichester, UK (1998)
56. Lie, K., Møyner, O., Natvig, J.R.: Use of Multiple Multiscale Operators To Accelerate Simulation of Complex Geomodels. *SPE J.* **22**(6), 1929–1945 (2017). DOI 10.2118/182701-PA
57. Lie, K., Møyner, O., Natvig, J.R., Kozlova, A., Bratvedt, K., Watanabe, S., Li, Z.: Successful Application of Multiscale Methods in a Real Reservoir Simulator Environment. In: *Proceedings of the 15th European Conference on the Mathematics of Oil Recovery (ECMOR XV)*. EAGE (2016). DOI 10.3997/2214-4609.201601893
58. Lipnikov, K.: *Numerical Methods for the Biot Model in Poroelasticity*. PhD thesis, University of Houston (2002)
59. Lunati, I., Tyagi, M., Lee, S.H.: An iterative multiscale finite volume algorithm converging to the exact solution. *J. Comput. Phys.* **230**(5), 1849–1864 (2011). DOI 10.1016/j.jcp.2013.11.024
60. Luo, P., Rodrigo, C., Gaspar, F.J., Oosterlee, C.W.: Multigrid method for nonlinear poroelasticity equations. *Comput. Visual Sci.* **17**(5), 255–265 (2015). DOI 10.1007/s00791-016-0260-8
61. Luo, P., Rodrigo, C., Gaspar, F.J., Oosterlee, C.W.: On an Uzawa smoother in multigrid for poroelasticity equations. *Numer. Linear Algebr. Appl.* **24**(1), e2074 (2017). DOI 10.1002/nla.2074
62. Meijerink, J.A., van der Vorst, H.A.: An iterative solution method for linear systems of which the coefficient matrix is a symmetric M -matrix. *Math. Comput.* **31**(137), 148–162 (1977). DOI 10.1090/S0025-5718-1977-0438681-4
63. Mikelic, A., Wheeler, M.F.: Convergence of iterative coupling for coupled flow and geomechanics. *Comput. Geosci.* **17**(3), 455–461 (2013). DOI 10.1007/s10596-012-9318-y
64. Møyner, O., Lie, K.: A multiscale restriction-smoothed basis method for high contrast porous media represented on unstructured grids. *J. Comput. Phys.* **304**, 46–71 (2016). DOI 10.1016/j.jcp.2015.10.010
65. Murad, M.A., Loula, A.F.D.: On stability and convergence of finite element approximations of Biot's consolidation problem. *Int. J. Numer. Meth. Eng.* **37**(4), 645–667 (1994). DOI 10.1002/nme.1620370407
66. Nordbotten, J.M.: Cell-centered finite volume discretizations for deformable porous media. *Int. J. Numer. Meth. Eng.* **100**(6), 399–418 (2014). DOI 10.1002/nme.4734
67. Nordbotten, J.M.: Stable Cell-Centered Finite Volume Discretization for Biot Equations. *SIAM J. Numer. Anal.* **54**(6), 942–968 (2016). DOI 10.1137/15M1014280
68. Nordbotten, J.M., Bjøstad, P.E.: On the relationship between the multiscale finite volume method and domain decomposition preconditioners. *Comput. Geosci.* **13**(3), 367–376 (2008). DOI 10.1007/s10596-007-9066-6
69. Pasetto, D., Ferronato, M., Putti, M.: A reduced order model-based preconditioner for the efficient solution of transient diffusion equations. *Int. J. Numer. Meth. Eng.* **n/a**, n/a–n/a (2016). DOI 10.1002/nme.5320
70. Phillips, P.J., Wheeler, M.F.: A coupling of mixed and continuous Galerkin finite element methods for poroelasticity I: the continuous in time case. *Comput. Geosci.* **11**(2), 131–144 (2007a). DOI 10.1007/s10596-007-9045-y
71. Phillips, P.J., Wheeler, M.F.: A coupling of mixed and continuous Galerkin finite element methods for poroelasticity II: the discrete-in-time case. *Comput. Geosci.* **11**(2), 145–158 (2007b). DOI 10.1007/s10596-007-9044-z
72. Prevost, J.H.: Twoway coupling in reservoirgeomechanical models: vertexcentered Galerkin geomechanical model cellcentered and vertexcentered finite volume reservoir models. *Int. J. Numer. Meth. Eng.* **98**(2), 612–624 (2014). DOI 10.1002/nme.4657
73. Rodrigo, C., Gaspar, F., Hu, X., Zikatanov, L.: Stability and monotonicity for some discretizations of the Biot's consolidation model. *Comput. Meth. Appl. Mech. Eng.* **298**, 183–204 (2016). DOI 10.1016/j.cma.2015.09.019

74. Rodrigo, C., Hu, X., Ohm, P., Adler, J.H., Gaspar, F.J., Zikatanov, L.: New stabilized discretizations for poroelasticity and the Stokes' equations (2018). DOI 10.1016/j.cma.2018.07.003
75. Saad, Y.: Iterative Methods for Sparse Linear Systems, 2nd edn. Society for Industrial and Applied Mathematics, Philadelphia, PA, USA (2003). DOI 10.1137/1.9780898718003
76. Saad, Y., Schultz, M.H.: GMRES: A Generalized Minimal Residual Algorithm for Solving Nonsymmetric Linear Systems. *SIAM J. Sci. Stat. Comput.* **7**(3), 856–869 (1986). DOI 10.1137/0907058
77. Schneider, M., Flemisch, B., Helmig, R., Terekhov, K., Tchelepi, H.A.: Monotone nonlinear finite-volume method for challenging grids. *Comput. Geosci.* (2018). DOI 10.1007/s10596-017-9710-8
78. Settari, A., Mourits, F.M.: A Coupled Reservoir and Geomechanical Simulation System. *SPE J.* **3**(3), 219–226 (1998). DOI {10.2118/50939-PA}
79. Spillane, N., Dolean, V., Hauret, P., Nataf, F., Pechstein, C., Scheichl, R.: Abstract robust coarse spaces for systems of PDEs via generalized eigenproblems in the overlaps. *Numer. Math.* **126**(4), 741–770 (2014). DOI 10.1007/s00211-013-0576-y
80. Tene, M., Al Kobaisi, M.S., Hajibeygi, H.: Algebraic Multiscale Method for Fractured Porous Media. *J. Comput. Phys.* **321**, 819–845 (2016). DOI 10.1016/j.jcp.2016.06.012
81. Tene, M., Wang, Y., Hajibeygi, H.: Algebraic Multiscale Method for Fractured Porous Media. *J. Comput. Phys.* **300**, 679–694 (2015). DOI 10.1016/j.jcp.2015.08.009
82. Terekhov, K.M., Mallison, B.T., Tchelepi, H.A.: Cell-centered nonlinear finite-volume methods for the heterogeneous anisotropic diffusion problem. *J. Comput. Phys.* **330**, 245–267 (2017). DOI 10.1016/j.jcp.2016.11.010
83. Turan, E., Arbenz, P.: Large scale micro finite element analysis of 3D bone poroelasticity. *Parallel Comput.* **40**(7), 239–250 (2014). DOI 10.1016/j.parco.2013.09.002
84. Wang, H.F.: Theory of Linear Poroelasticity. Princeton University Press, Princeton, NJ, USA (2000)
85. Wang, Y., Hajibeygi, H., Tchelepi, H.A.: Algebraic multiscale solver for flow in heterogeneous porous media. *J. Comput. Phys.* **259**, 284–303 (2014). DOI 10.1016/j.jcp.2013.11.024
86. Wang, Y., Hajibeygi, H., Tchelepi, H.A.: Monotone multiscale finite volume method. *Comput. Geosci.* **20**, 509–524 (2016). DOI 10.1007/s10596-015-9506-7
87. White, J.A., Borja, R.: Block-preconditioned Newton–Krylov solvers for fully coupled flow and geomechanics. *Comput. Geosci.* **15**(4), 647–659 (2011). DOI 10.1007/s10596-011-9233-7
88. White, J.A., Borja, R.I.: Stabilized low-order finite elements for coupled solid-deformation/fluid-diffusion and their application to fault zone transients. *Comput. Meth. Appl. Mech. Eng.* **197**(49–50), 4353–4366 (2008). DOI 10.1016/j.cma.2008.05.015
89. White, J.A., Castelletto, N., Tchelepi, H.A.: Block-partitioned solvers for coupled poromechanics: A unified framework. *Comput. Meth. Appl. Mech. Eng.* **303**, 55–74 (2016). DOI 10.1016/j.cma.2016.01.008
90. Yi, S.Y.: Convergence analysis of a new mixed finite element method for Biot's consolidation model. *Numer. Meth. Part. Differ. Equ.* **30**(4), 1189–1210 (2014). DOI 10.1002/num.21865
91. Zhang, H.W., Fu, Z.D., Wu, J.K.: Coupling multiscale finite element method for consolidation analysis of heterogeneous saturated porous media. *Adv. Water Resour.* **32**(2), 268–279 (2009). DOI 10.1016/j.advwatres.2008.11.002
92. Zhou, H., Tchelepi, H.A.: Two-Stage Algebraic Multiscale Linear Solver for Highly Heterogeneous Reservoir Models. *SPE J.* **17**(2), 523–539 (2012). DOI 10.2118/141473-PA